

# Analysis of Texture and Oriented Patterns in Biomedical Images

Rangaraj M. Rangayyan

Professor Emeritus of Electrical and Computer Engineering  
University of Calgary, Alberta, Canada

Contains material from R.M. Rangayyan,  
“Biomedical Image Analysis,” © CRC Press, 2005



**UNIVERSITY OF  
CALGARY**



# Detection and Analysis of Regions in Images

After regions of interest (ROIs) have been detected and extracted from a given image, they may be analyzed for

- ❖ representation or characterization
- ❖ description
- ❖ feature extraction
- ❖ pattern classification and
- ❖ image understanding



# Description of Regions

- ❖ External characteristics:
  - boundary or contour morphology (shape)
  - boundary roughness and sharpness
  - boundary complexity
- ❖ Internal characteristics:
  - gray level
  - color
  - statistics of pixel population
  - **texture**

# Examples of Texture

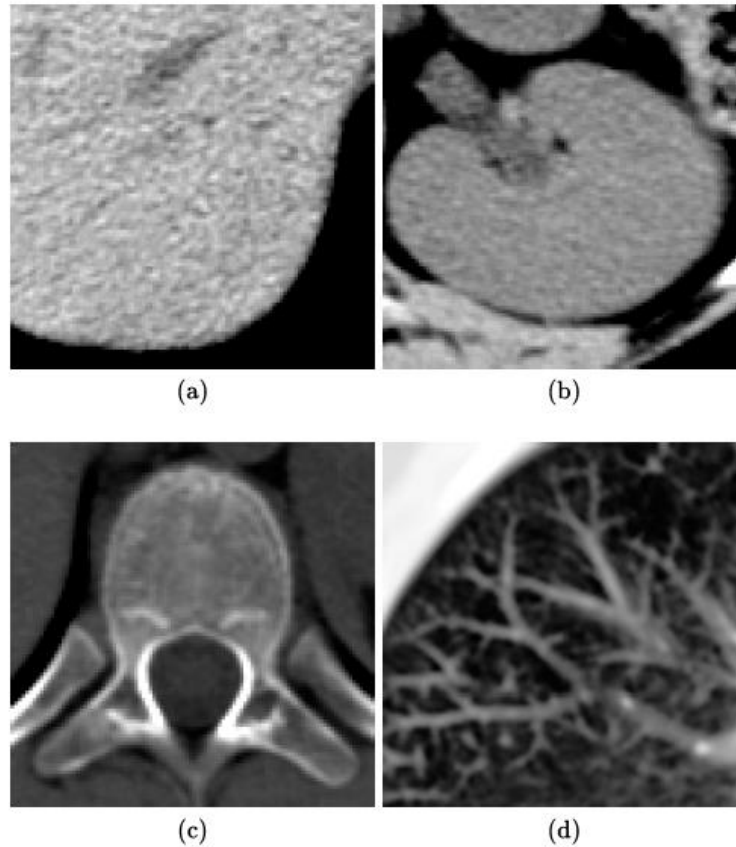


**FIGURE 7.1**

Examples of texture in CT images: (a) Liver. (b) Kidney. (c) Spine. (d) Lung. The true size of each image is  $55 \times 55$  mm. The images represent widely differing ranges of tissue density, and have been enhanced to display the inherent texture. Image data courtesy of Alberta Children's Hospital.

# Examples of Texture

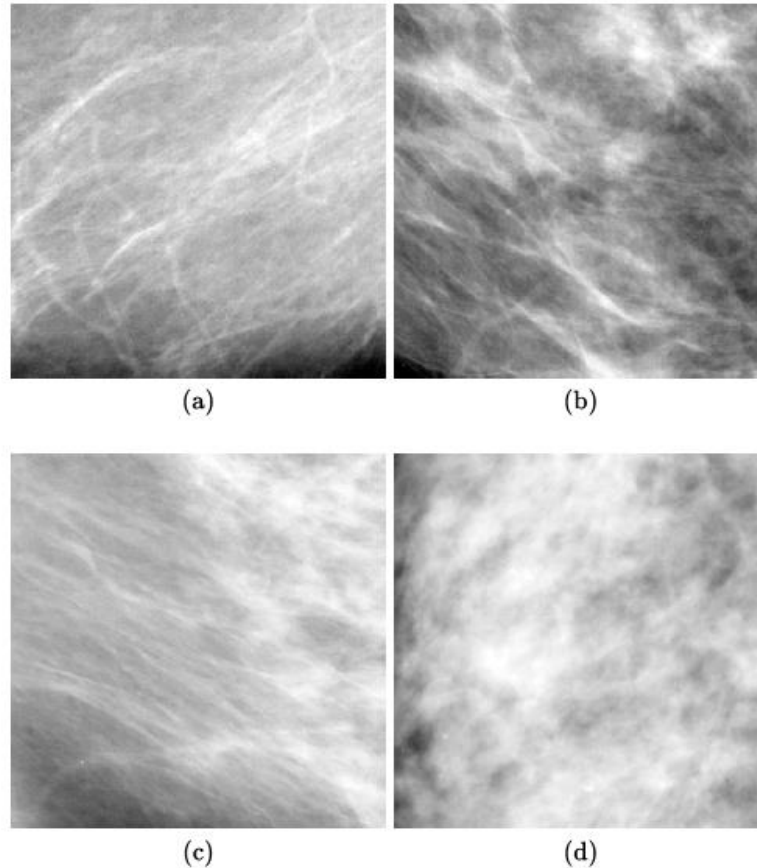


**FIGURE 7.2**

Examples of texture in mammograms (from the MIAS database [376]): (a) – (c) oriented texture; true image size  $60 \times 60$  mm; (d) random texture; true image size  $40 \times 40$  mm. For more examples of oriented texture, see Figures 9.20 and 1.8, as well as Chapter 8.

# Examples of Texture

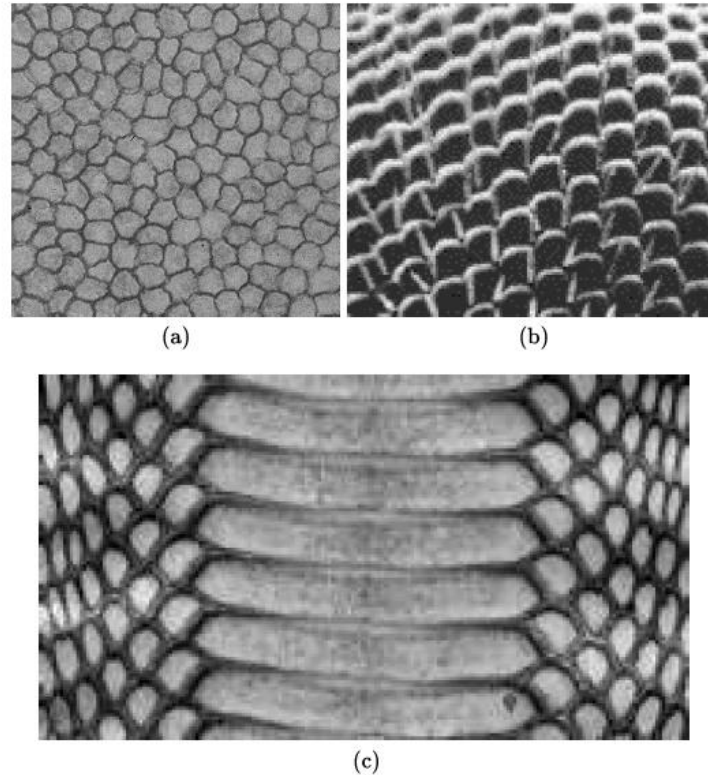
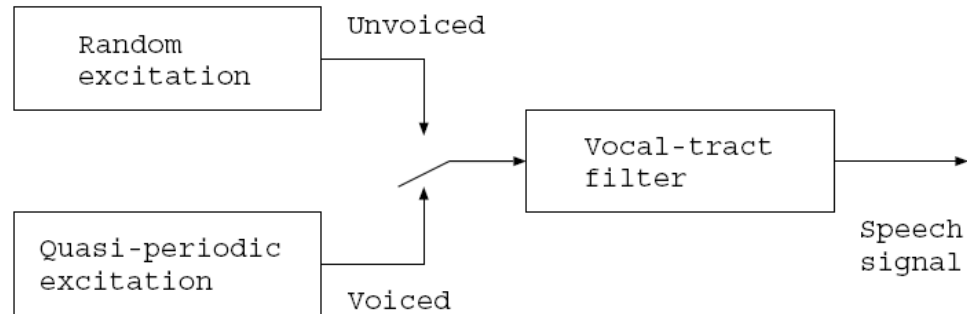


**FIGURE 7.3**

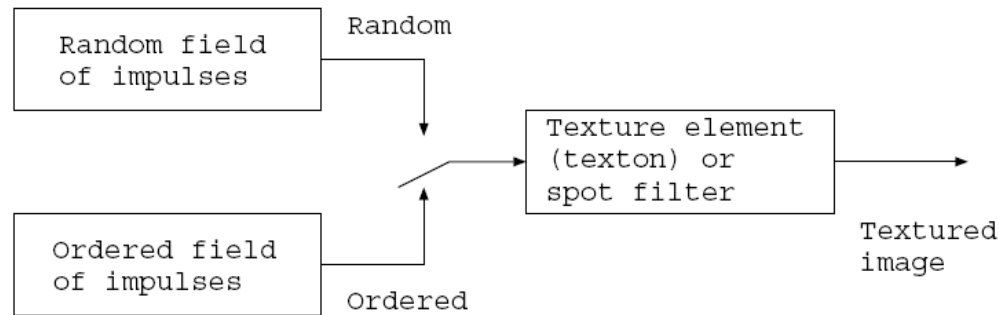
Examples of ordered texture: (a) Endothelial cells in the cornea. Image courtesy of J. Jaroszewski. (b) Part of a fly's eye. Reproduced with permission from D. Suzuki, "Behavior in drosophila melanogaster: A geneticist's view", *Canadian Journal of Genetics and Cytology*, XVI(4): 713 – 735, 1974. © Genetics Society of Canada. (c) Skin on the belly of a cobra snake. Image courtesy of Implora, Colonial Heights, VA. <http://www.implora.com>. See also Figure 1.5.



# Models for the Synthesis of Texture



(a)



(b)

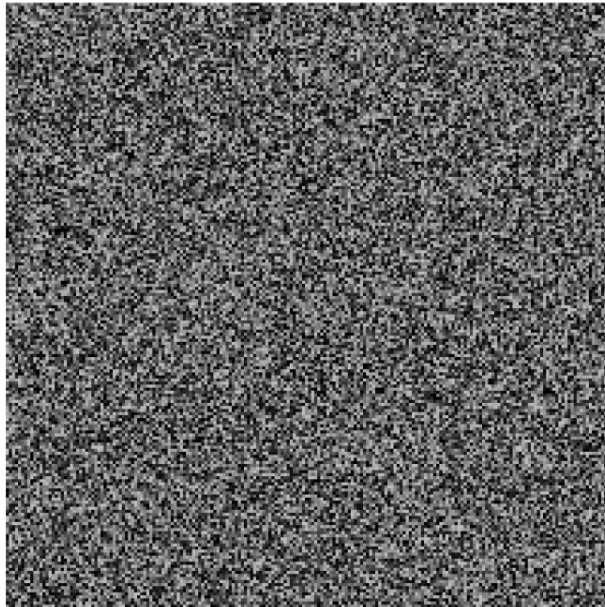
**FIGURE 7.4**

(a) Model for speech signal generation. (b) Model for texture synthesis.

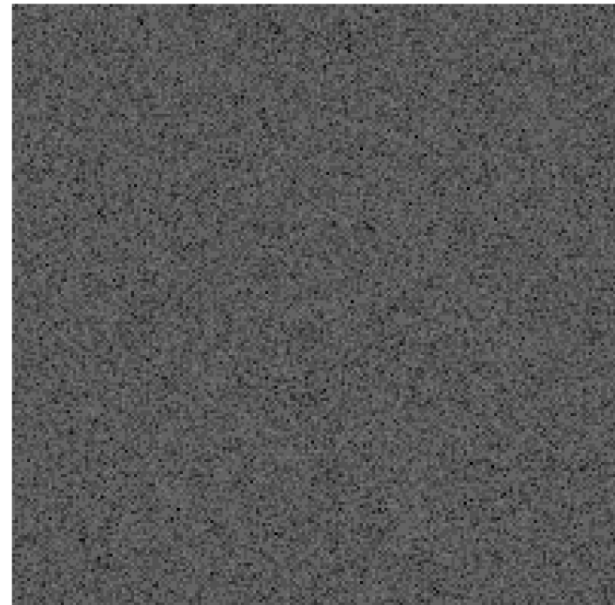


UNIVERSITY OF  
CALGARY

# Synthesis of Random Texture: Spot Noise



(a)



(b)

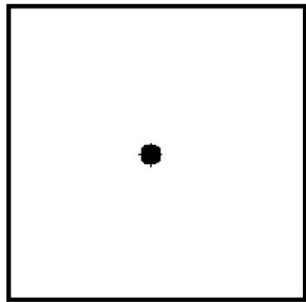
**FIGURE 7.5**

(a) Image of a random-noise field ( $256 \times 256$  pixels). (b) Spectrum of the image in (a). Reproduced with permission from A.C.G. Martins, R.M. Rangayyan, and R.A. Ruschioni, “Audification and sonification of texture in images”, *Journal of Electronic Imaging*, 10(3): 690 – 705, 2001. © SPIE and IS&T.

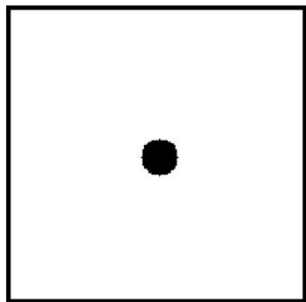




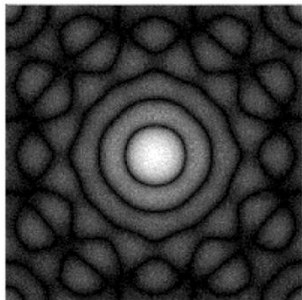
# Synthesis of Random Texture: Spot Noise



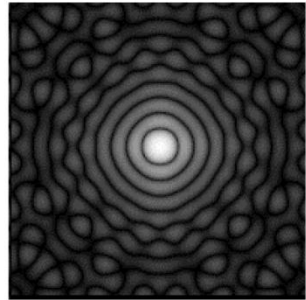
(a)



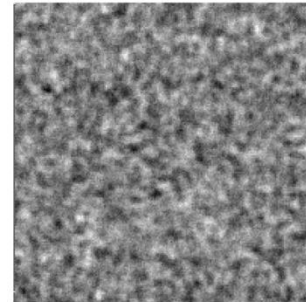
(b)



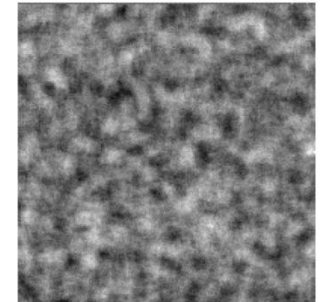
(c)



(d)



(e)



(f)

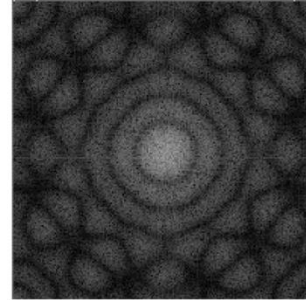
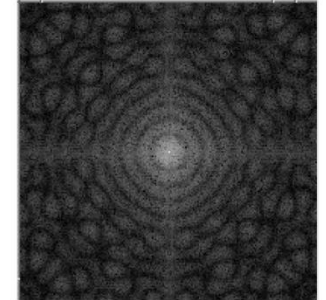


Figure 7.6 (g)



(h)

**FIGURE 7.6**

(a) Circle of diameter 12 pixels. (b) Circle of diameter 20 pixels. (c) Fourier spectrum of the image in (a). (d) Fourier spectrum of the image in (b). (e) Random texture with the circle of diameter 12 pixels as the spot. (f) Random texture with the circle of diameter 20 pixels as the spot. (g) Fourier spectrum of the image in (e). (h) Fourier spectrum of the image in (f). The size of each image is  $256 \times 256$  pixels. Reproduced with permission from A.C.G. Martins, R.M. Rangayyan, and R.A. Ruschioni, "Audification and sonification of texture in images", *Journal of Electronic Imaging*, 10(3): 690 – 705, 2001. © SPIE and IS&T.



UNIVERSITY OF  
CALGARY

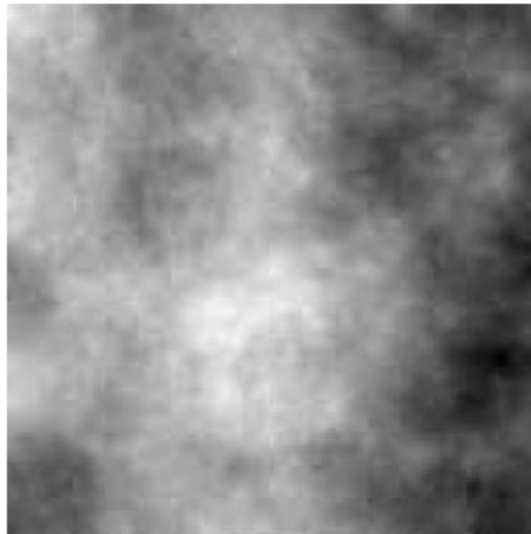
# Fractals

Self Similarity:  
repetition at  
multiple scales

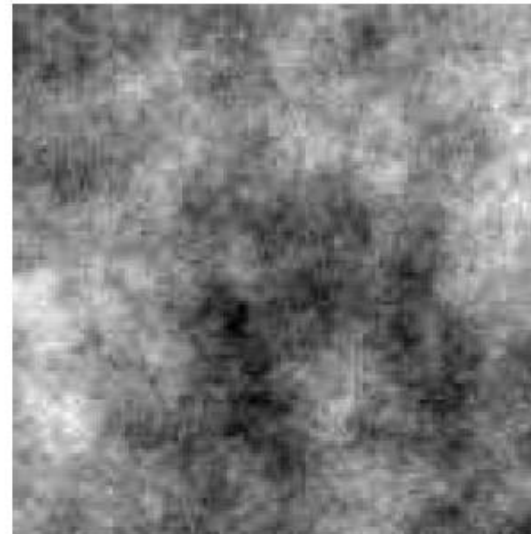




# Fractional Brownian Motion and $1/f$ Models of Fractals



(a)



(b)

Examples of two synthetic ROIs with known FD. Each ROI is of size  $128 \times 128$  pixels.  
(a) True FD = 2.30, estimated FD = 2.38. (b) True FD = 2.70, estimated FD = 2.76.



# Analysis of Texture

## 7.3 Statistical Analysis of Texture

Simple measures of texture may be derived based upon the moments of the gray-level PDF (or normalized histogram) of the given image. The  $k^{\text{th}}$  central moment of the PDF  $p(l)$  is defined as

$$m_k = \sum_{l=0}^{L-1} (l - \mu_f)^k p(l), \quad (7.1)$$

where  $l = 0, 1, 2, \dots, L - 1$  are the gray levels in the image  $f$ , and  $\mu_f$  is the mean gray level of the image given by

$$\mu_f = \sum_{l=0}^{L-1} l p(l). \quad (7.2)$$



# Analysis of Texture

The second central moment, which is the variance of the gray levels and is given by

$$\sigma_f^2 = m_2 = \sum_{l=0}^{L-1} (l - \mu_f)^2 p(l), \quad (7.3)$$

can serve as a measure of inhomogeneity. The normalized third and fourth moments, known as the skewness and kurtosis, respectively, and defined as

$$\text{skewness} = \frac{m_3}{m_2^{3/2}}, \quad (7.4)$$

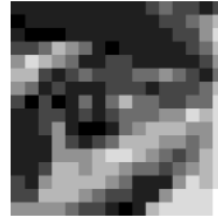
and

$$\text{kurtosis} = \frac{m_4}{m_2^2}, \quad (7.5)$$

indicate the asymmetry and uniformity (or lack thereof) of the PDF.



# Derivation of the Gray-level Cooccurrence Matrix



1	1	1	1	1	1	1	1	1	1	2	3	2	2	1	2
0	1	1	1	1	1	1	1	1	1	1	2	2	3	4	5
1	0	0	0	1	1	1	1	1	1	1	1	2	2	4	6
2	2	3	5	4	3	1	0	1	1	1	1	1	2	3	5
4	6	5	4	3	1	1	2	2	1	1	1	1	1	2	4
5	5	2	1	2	3	2	2	2	3	3	4	3	2	1	3
4	3	1	2	1	1	1	2	2	2	1	2	2	2	3	5
2	0	2	0	1	3	1	3	5	3	3	2	2	3	3	6
1	1	2	2	1	2	1	2	3	3	3	4	4	6	5	6
1	1	2	4	1	0	0	1	3	4	5	5	5	4	4	6
1	1	1	4	2	1	2	3	5	5	5	4	4	3	4	6
1	1	1	4	4	4	5	6	6	5	4	3	2	3	5	6
1	1	2	5	5	4	5	5	4	3	3	2	3	4	5	6
2	1	4	5	5	5	5	4	3	1	1	1	4	6	5	6
2	2	5	5	5	4	3	2	2	1	1	4	6	6	6	7
4	4	4	4	3	2	2	1	0	1	5	6	6	6	6	7

**FIGURE 7.11**

A  $16 \times 16$  part of the image in Figure 2.1 (a) quantized to  $3 \text{ b/pixel}$ , shown as an image and as a 2D array of pixel values.



# The Gray-level Cooccurrence Matrix

**TABLE 7.1**

Gray-level Co-occurrence Matrix for the Image in Figure 7.11, with the Second Pixel Immediately Below the First.

Current Pixel	Next Pixel Below							
	0	1	2	3	4	5	6	7
0	0	3	4	1	0	1	0	0
1	6	44	10	9	5	1	0	0
2	3	13	13	5	8	3	1	0
3	1	5	11	5	3	5	2	0
4	0	1	5	7	5	9	3	0
5	0	0	1	5	11	10	4	0
6	0	0	0	0	2	3	10	1
7	0	0	0	0	0	0	0	1



# Analysis of Texture using the GCM

## 7.3.2 Haralick's measures of texture

Based upon normalized GCMs, Haralick et al. [441, 442] proposed several quantities as measures of texture. In order to define these measures, let us normalize the GCM as

$$p(l_1, l_2) = \frac{P(l_1, l_2)}{\sum_{l_1=0}^{L-1} \sum_{l_2=0}^{L-1} P(l_1, l_2)}. \quad (7.6)$$





# Analysis of Texture using the GCM

A few other entities used in the derivation of Haralick's texture measures are as follows:

$$p_x(l_1) = \sum_{l_2=0}^{L-1} p(l_1, l_2), \quad (7.7)$$

$$p_y(l_2) = \sum_{l_1=0}^{L-1} p(l_1, l_2), \quad (7.8)$$

$$p_{x+y}(k) = \underbrace{\sum_{l_1=0}^{L-1} \sum_{l_2=0}^{L-1} p(l_1, l_2)}_{l_1+l_2=k}, \quad (7.9)$$

where  $k = 0, 1, 2, \dots, 2(L - 1)$ , and

$$p_{x-y}(k) = \underbrace{\sum_{l_1=0}^{L-1} \sum_{l_2=0}^{L-1} p(l_1, l_2)}_{|l_1-l_2|=k}, \quad (7.10)$$

where  $k = 0, 1, 2, \dots, L - 1$ .



# Analysis of Texture using the GCM

The energy feature  $F_1$ , which is a measure of homogeneity, is defined as

$$F_1 = \sum_{l_1=0}^{L-1} \sum_{l_2=0}^{L-1} p^2(l_1, l_2). \quad (7.11)$$

A homogeneous image has a small number of entries along the diagonal of the GCM with large values, which will lead to a large value of  $F_1$ . On the other hand, an inhomogeneous image will have small values spread over a larger number of GCM entries, which will result in a low value for  $F_1$ .



# Analysis of Texture using the GCM

The contrast feature  $F_2$  is defined as

$$F_2 = \sum_{k=0}^{L-1} k^2 \underbrace{\sum_{l_1=0}^{L-1} \sum_{l_2=0}^{L-1} p(l_1, l_2)}_{|l_1 - l_2| = k}. \quad (7.12)$$



# Analysis of Texture using the GCM

The correlation measure  $F_3$ , which represents linear dependencies of gray levels, is defined as

$$F_3 = \frac{1}{\sigma_x \sigma_y} \left[ \sum_{l_1=0}^{L-1} \sum_{l_2=0}^{L-1} l_1 l_2 p(l_1, l_2) - \mu_x \mu_y \right], \quad (7.13)$$

where  $\mu_x$  and  $\mu_y$  are the means, and  $\sigma_x$  and  $\sigma_y$  are the standard deviations of  $p_x$  and  $p_y$ , respectively.

The sum of squares feature is given by

$$F_4 = \sum_{l_1=0}^{L-1} \sum_{l_2=0}^{L-1} (l_1 - \mu_f)^2 p(l_1, l_2), \quad (7.14)$$

where  $\mu_f$  is the mean gray level of the image.



# Analysis of Texture using the GCM

The inverse difference moment, a measure of local homogeneity, is defined as

$$F_5 = \sum_{l_1=0}^{L-1} \sum_{l_2=0}^{L-1} \frac{1}{1 + (l_1 - l_2)^2} p(l_1, l_2). \quad (7.15)$$

The sum average feature  $F_6$  is given by

$$F_6 = \sum_{k=0}^{2(L-1)} k p_{x+y}(k), \quad (7.16)$$

and the sum variance feature  $F_7$  is defined as

$$F_7 = \sum_{k=0}^{2(L-1)} (k - F_6)^2 p_{x+y}(k). \quad (7.17)$$



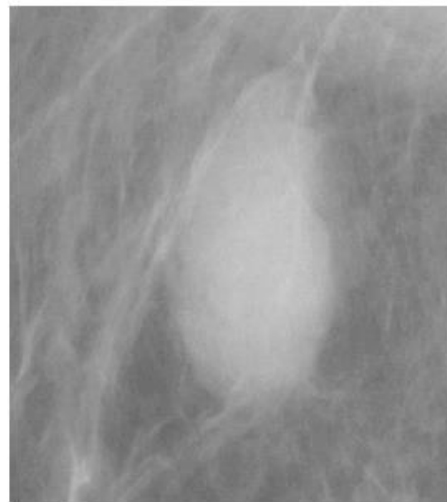
# Analysis of Texture using the GCM

The sum entropy feature  $F_8$  is given by

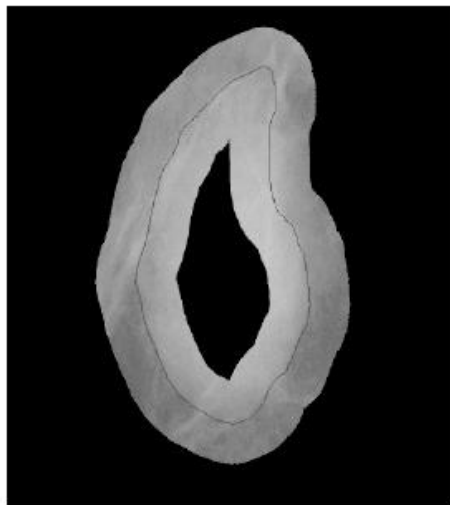
$$F_8 = - \sum_{k=0}^{2(L-1)} p_{x+y}(k) \log_2 [p_{x+y}(k)]. \quad (7.18)$$

Entropy, a measure of nonuniformity in the image or the complexity of the texture, is defined as

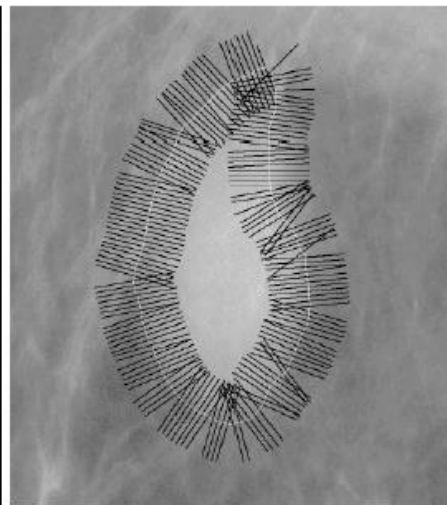
$$F_9 = - \sum_{l_1=0}^{L-1} \sum_{l_2=0}^{L-1} p(l_1, l_2) \log_2 [p(l_1, l_2)]. \quad (7.19)$$



(a)



(b)



(c)

**FIGURE 7.24**

(a) A  $1,000 \times 900$  section of a mammogram containing a circumscribed benign mass. Pixel size =  $50 \mu m$ . (b) Ribbon or band of pixels across the boundary of the mass extracted by using morphological operations. (c) Pixels along the normals to the boundary, shown for every tenth boundary pixel. Maximum length of the normals on either side of the boundary = 80 pixels or 4 mm.

*Extraction of regions of interest or selected pixels for the computation of texture and gradient measures*

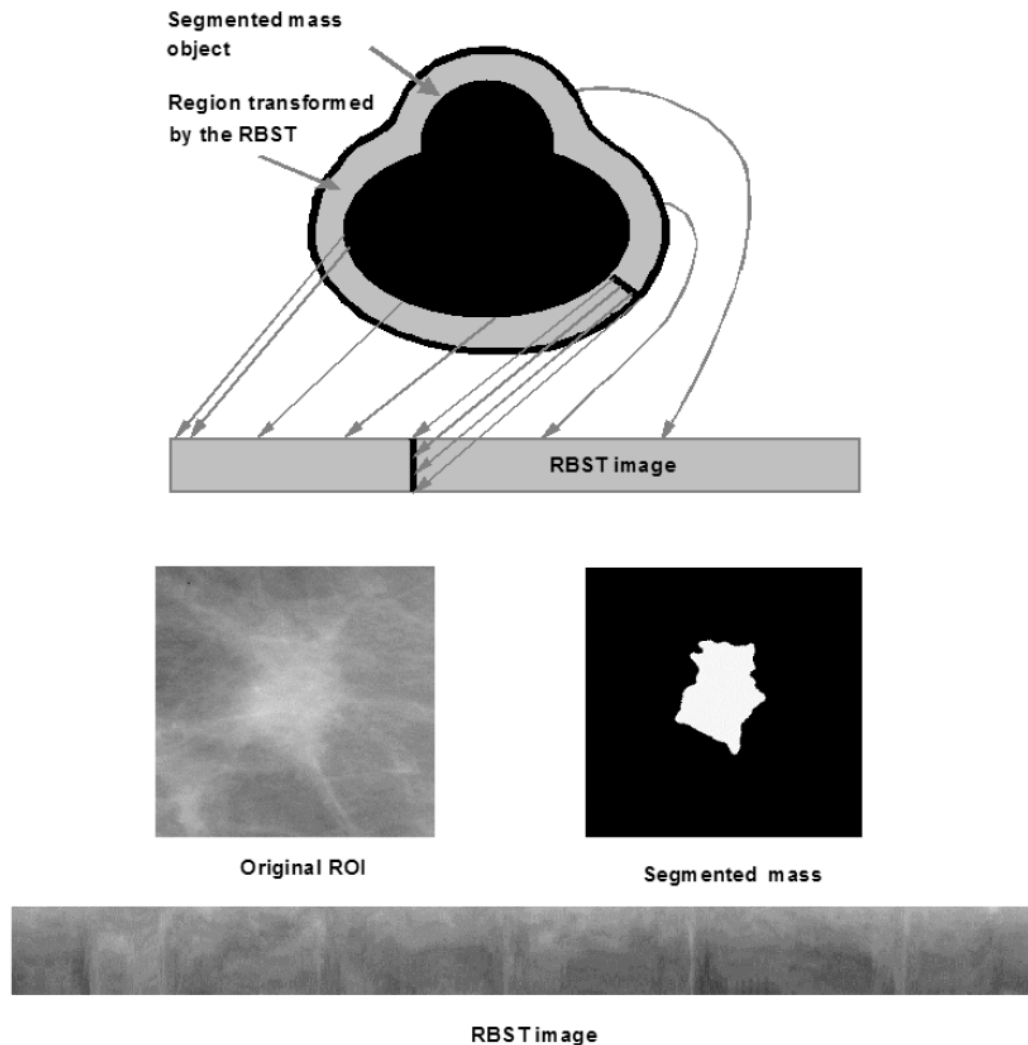


**FIGURE 7.26**

Mapping of a ribbon of pixels around a mass into a rectangular image by the rubber-band straightening transform [428, 451]. Figure courtesy of B. Sahiner, University of Michigan, Ann Arbor, MI. Reproduced with permission from B.S. Sahiner, H.P. Chan, N. Petrick, M.A. Helvie, and M.M. Goodsitt, "Computerized characterization of masses on mammograms: The rubber band straightening transform and texture analysis", *Medical Physics*, 25(4): 516 – 526, 1995. © American Association of Medical Physicists.





# Fourier Spectral Analysis of Texture

Let  $F(r, t)$  be the polar-coordinate representation of the Fourier spectrum of the given image; in terms of the Cartesian frequency coordinates  $(u, v)$ , we have  $r = \sqrt{u^2 + v^2}$ , and  $t = \text{atan}(v/u)$ . Derive the projection functions in  $r$  and  $t$  by integrating  $F(r, t)$  in the other coordinate as

$$F(r) = \int_{t=0}^{\pi} F(r, t) dt, \quad (7.40)$$

and

$$F(t) = \int_{r=0}^{r_{\max}} F(r, t) dr. \quad (7.41)$$

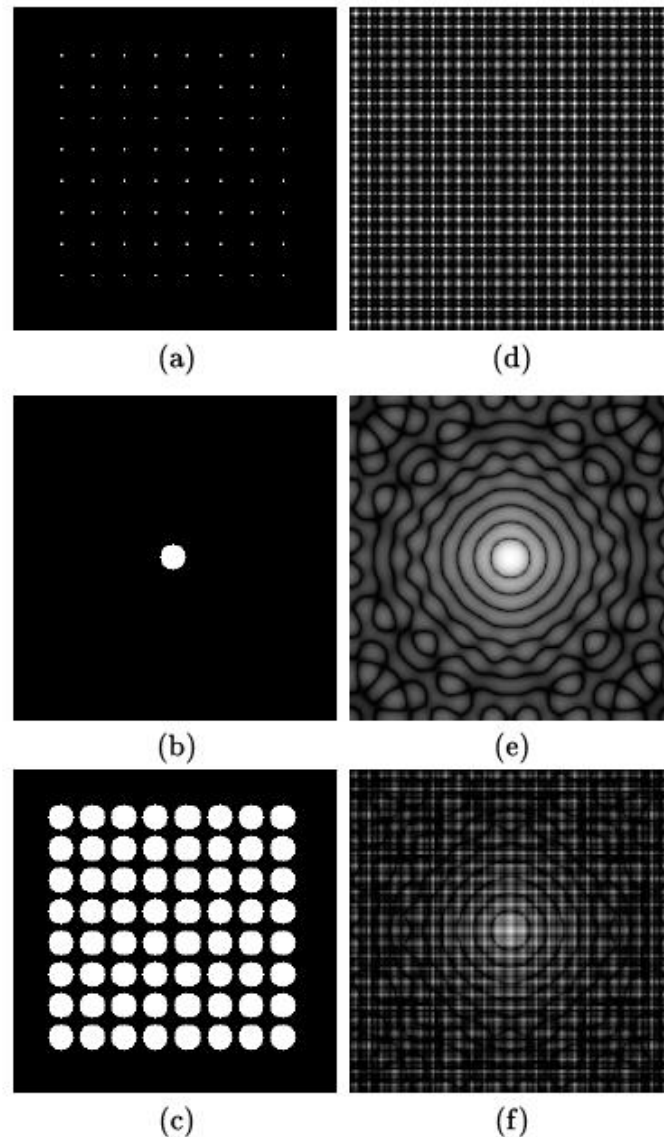


**FIGURE 7.15**

Fourier spectral characteristics of periodic texture generated using the spot-noise model in Figure 7.4. (a) Periodic impulse field. (b) Circular spot. (c) Periodic texture generated by convolving the spot in (b) with the impulse field in (a). (d) – (f) Log-magnitude Fourier spectra of the images in (a) – (c), respectively.

# Synthesis of Periodic Texture



# Fourier Spectrum in Polar Coordinates

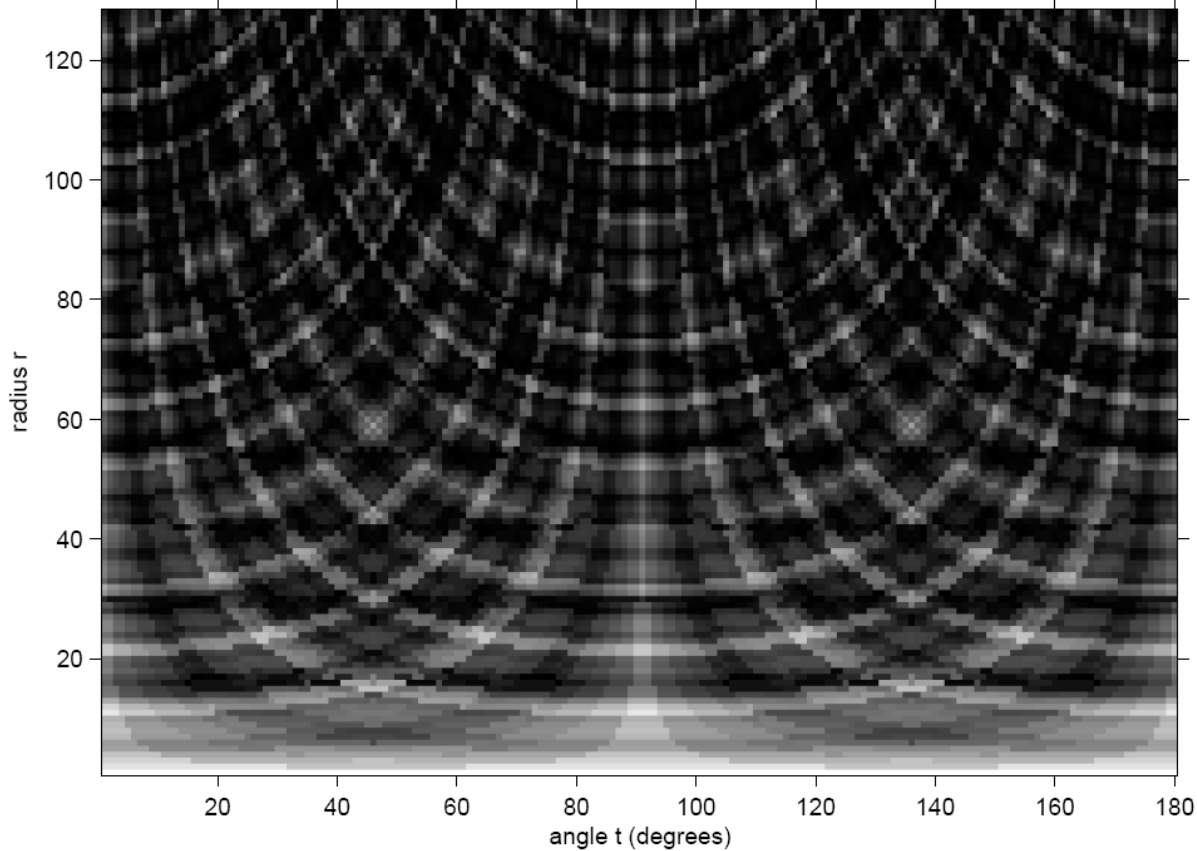
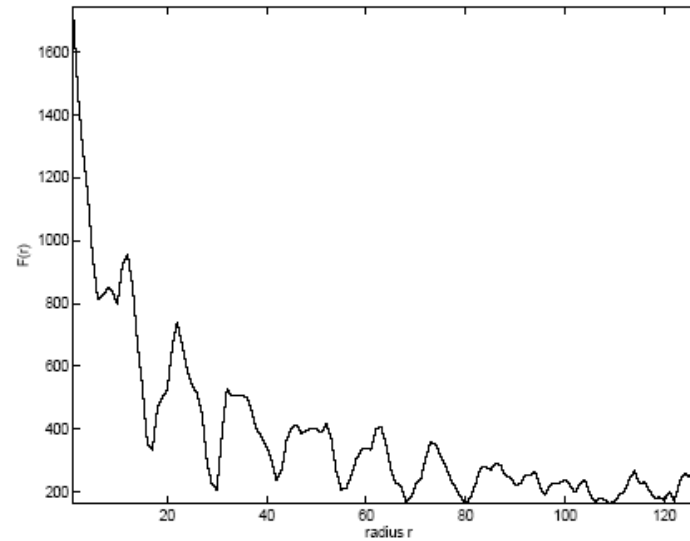
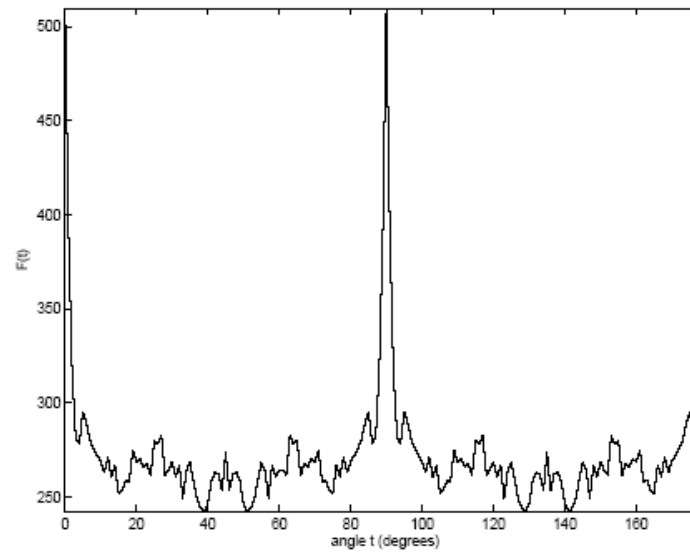


**FIGURE 7.16**

The spectrum in Figure 7.15 (f) converted to polar coordinates; only the upper half of the spectrum was mapped to polar coordinates.



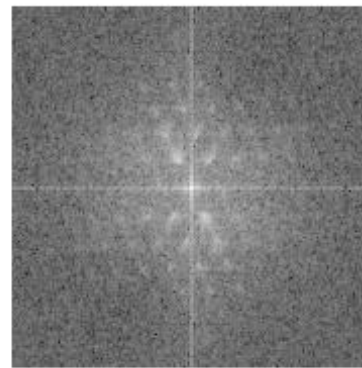
(a)



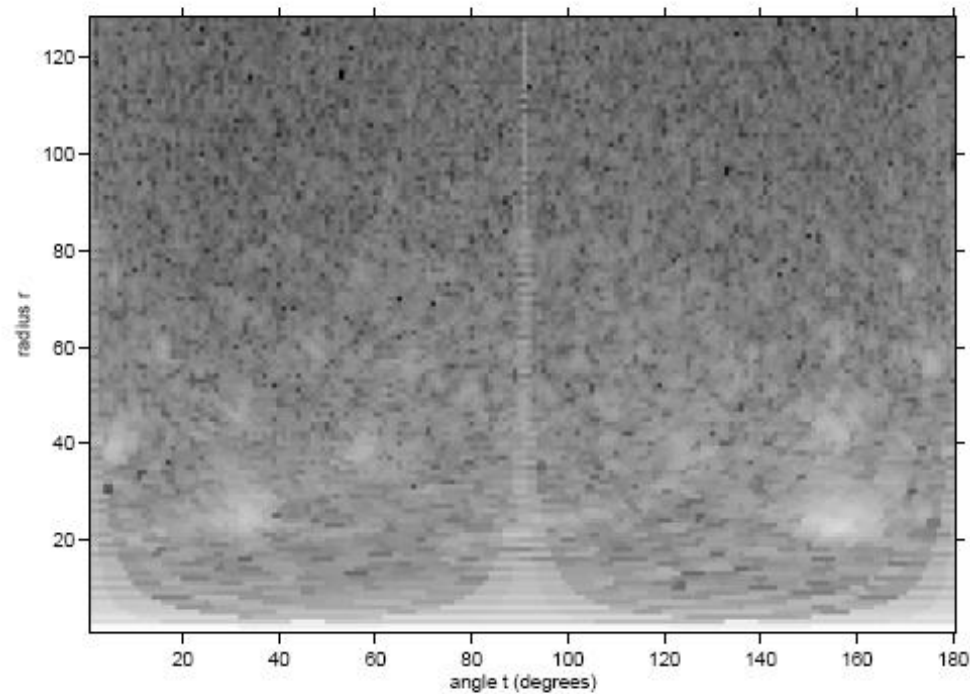
(b)

**FIGURE 7.17**

Projection functions in (a) the radial coordinate  $r$ , and (b) the angle coordinate  $t$  obtained by integrating (summing) the spectrum in Figure 7.16 in the other coordinate.



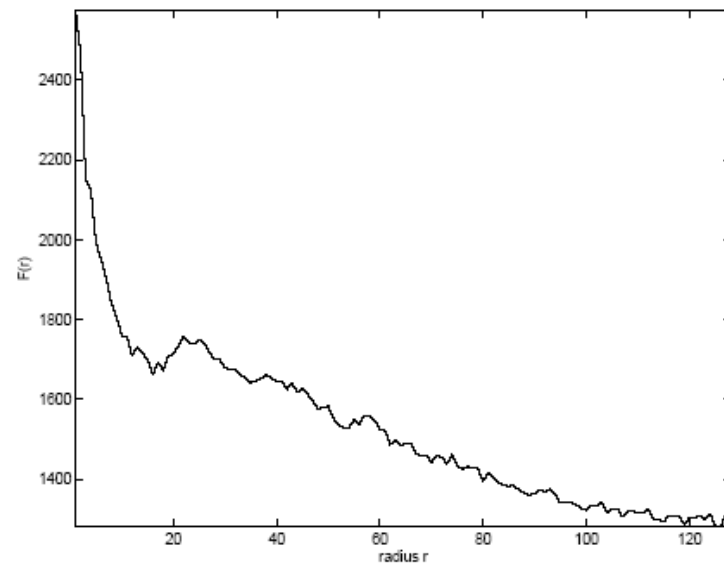
(a)



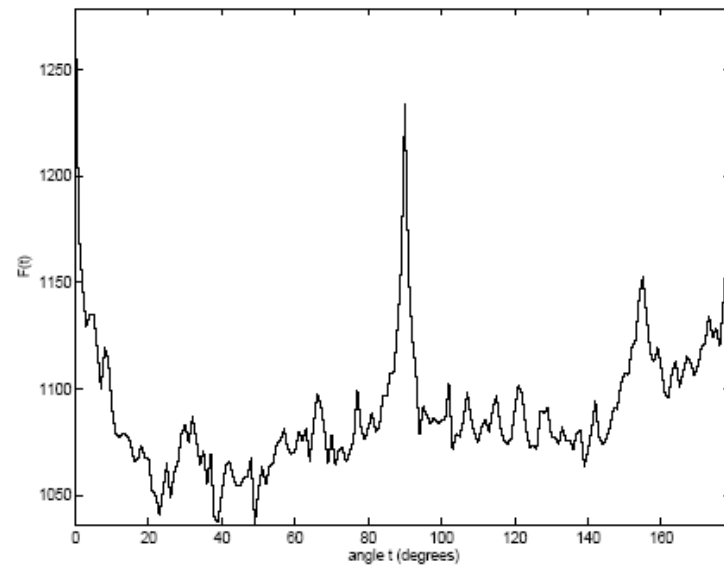
(b)

**FIGURE 7.18**

Fourier spectral characteristics of the quasi-periodic texture of the fly's eye image in Figure 7.3 (b): (a) The Fourier spectrum in Cartesian coordinates  $(u, v)$ . (b) The upper half of the spectrum in (a) mapped to polar coordinates.



(a)



(b)

**FIGURE 7.19**

Projection functions in (a) the radial coordinate  $r$ , and (b) the angle coordinate  $t$  obtained by integrating (summing) the spectrum in Figure 7.18 (b) in the other coordinate.



# Laws' Convolution Operators

- ❖ A method for classifying each pixel in an image based upon measures of local “texture energy”
- ❖ The texture energy features represent the amounts of gray-level variation within a sliding window
- ❖ The basic Laws' operators are:
  - $L3 = \begin{bmatrix} 1 & 2 & 1 \end{bmatrix}$  (center-weighted averaging)
  - $E3 = \begin{bmatrix} -1 & 0 & 1 \end{bmatrix}$  (edge detection)
  - $S3 = \begin{bmatrix} -1 & 2 & -1 \end{bmatrix}$  (spot detection)
- ❖ Nine  $3 \times 3$  masks can be generated by multiplying the transposes of the operators:  $L3^T E3 =$  a Sobel mask.



# Laws' Convolution Operators

- ❖ Operators of length five pixels may be generated by convolving  $L3$ ,  $E3$ , and  $S3$  in various combinations:

- $L5 = L3 * L3 = [ 1 \ 4 \ 6 \ 4 \ 1 ]$  (local average)

- $E5 = L3 * E3 = [ -1 \ -2 \ 0 \ 2 \ 1 ]$  (edges)

- $S5 = -E3 * E3 = [ -1 \ 0 \ 2 \ 0 \ -1 ]$  (spots)

- $R5 = -S3 * S3 = [ 1 \ -4 \ 6 \ -4 \ 1 ]$  (ripples)

- $W5 = -E3 * S3 = [ -1 \ 2 \ 0 \ -2 \ 1 ]$  (waves)

- ❖ Some  $5 \times 5$  convolution operators:

- $L5L5 = L5^T L5$

- $W5W5 = W5^T W5$

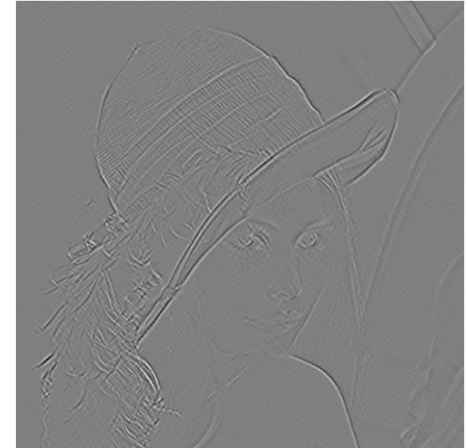
- $R5R5 = R5^T R5$





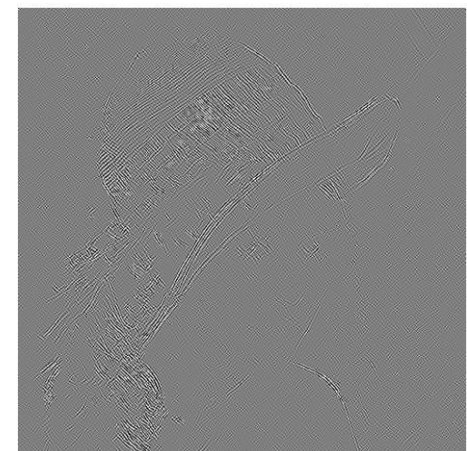
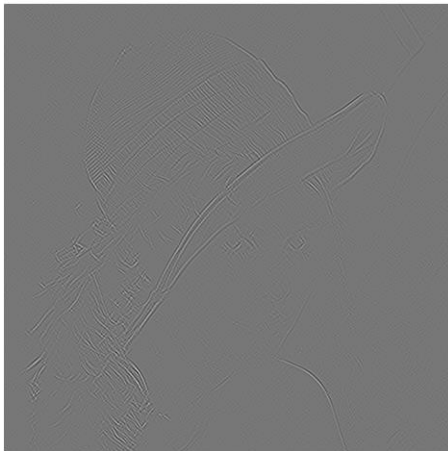
UNIVERSITY OF  
CALGARY

# Results of Laws' Operators



*L5L5*

*E5E5*



*S5S5*

*W5W5*

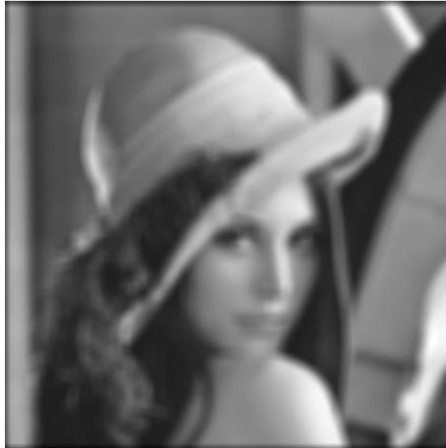
*R5R5*



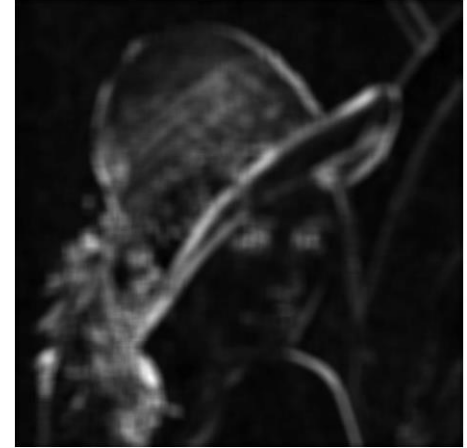
UNIVERSITY OF  
CALGARY

# Laws' Texture Energy Measures

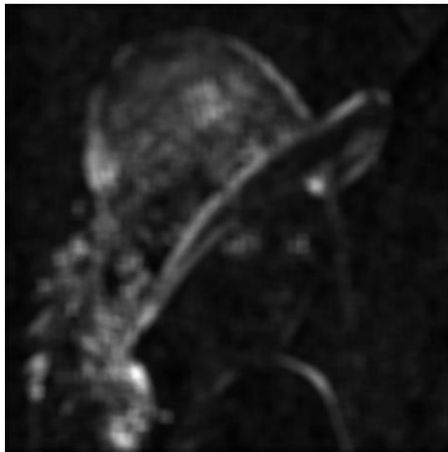
Sum of the absolute values in a  $15 \times 15$  window



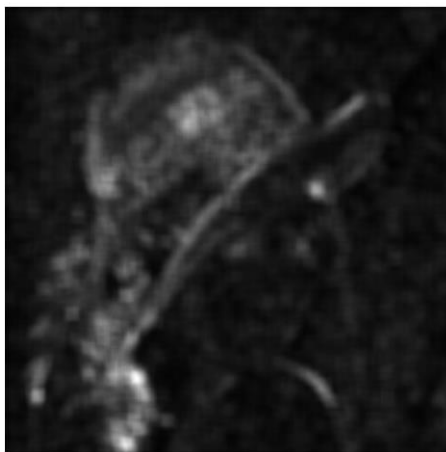
*L5L5*



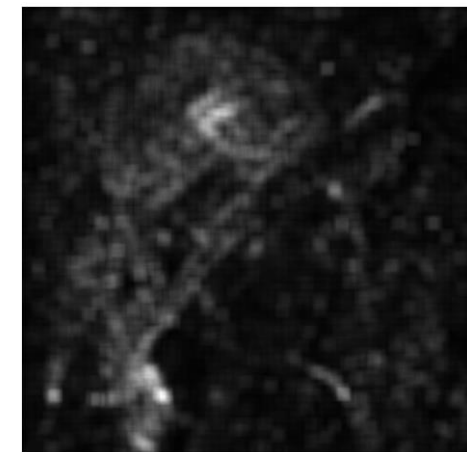
*E5E5*



*S5S5*



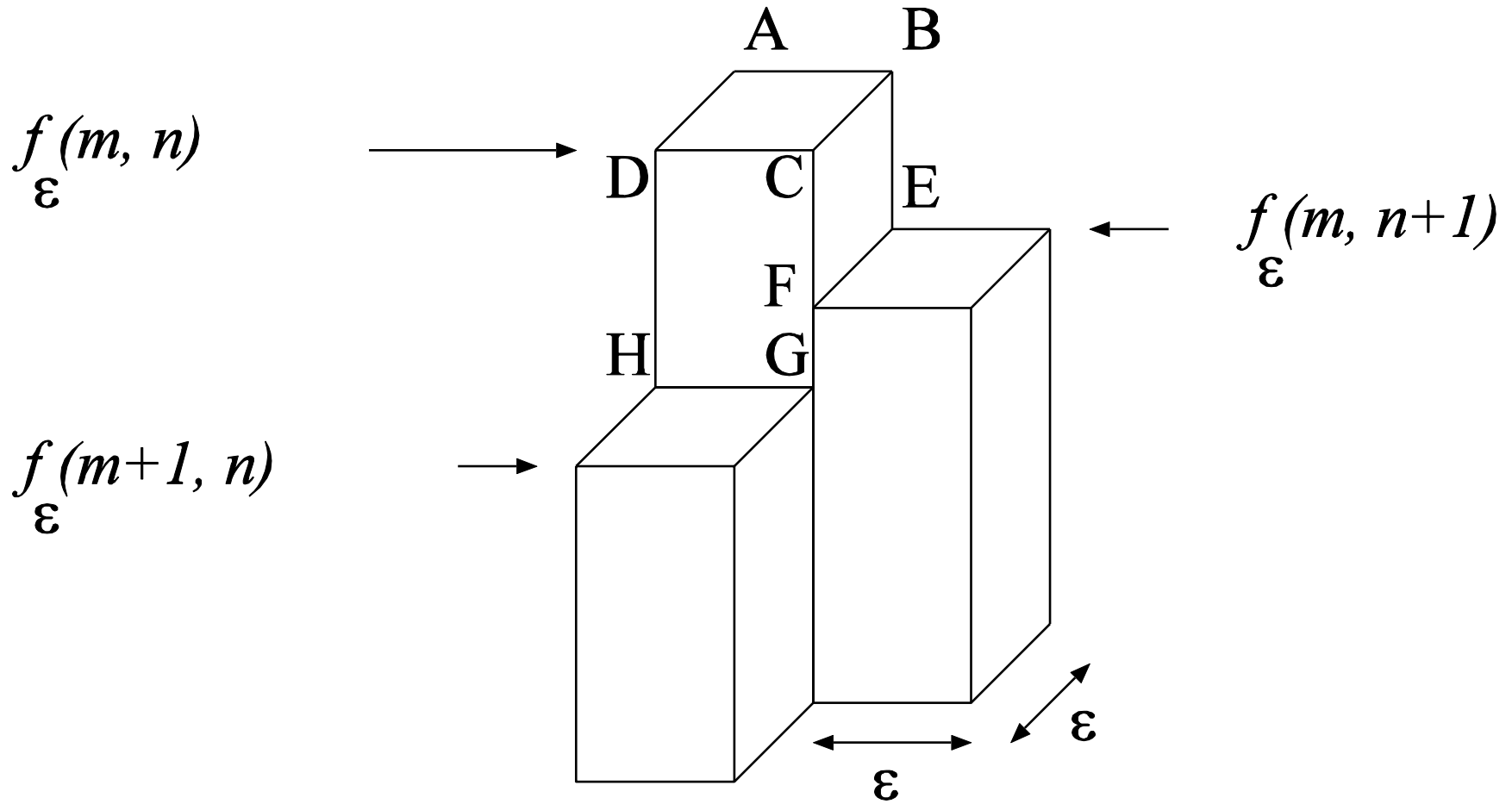
*W5W5*



*R5R5*



# Fractal Analysis of Grayscale Images: Blanket Method





# Fractal Analysis of Grayscale Images: Blanket Method

$$A(\varepsilon) = \sum_{m=0}^{N-2} \sum_{n=0}^{N-2} \{ \varepsilon^2 + \varepsilon [ |f_\varepsilon(m, n) - f_\varepsilon(m, n+1)| + |f_\varepsilon(m, n) - f_\varepsilon(m+1, n)| ] \}$$

$$D = 2 - \frac{\Delta \log[A(\varepsilon)]}{\Delta \log[\varepsilon]}$$



# Fractal Analysis of Grayscale Images: Spectral Method

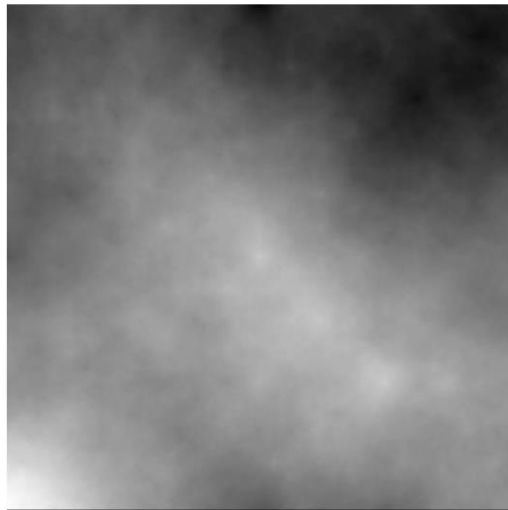
1. Compute the 2D Fourier transform of the image
2. Compute the 2D power spectral density (PSD)
3. Transform the 2D PSD into a 1D PSD by radial averaging
4. Fit a straight line to a selected range of frequencies of the 1D PSD on a log–log scale
5. Determine the slope  $\beta$  of the best-fitting straight line

$$FD = \frac{8 - \beta}{2}$$

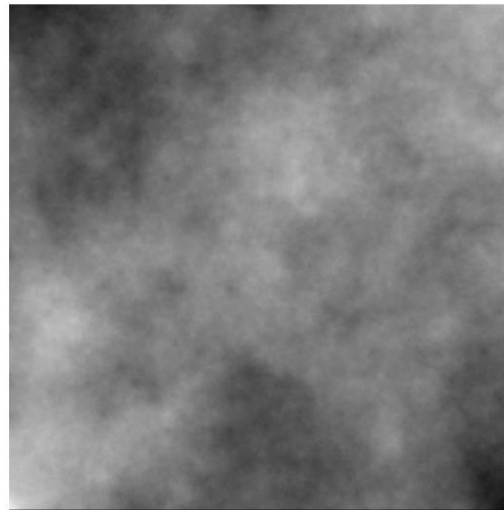


UNIVERSITY OF  
CALGARY

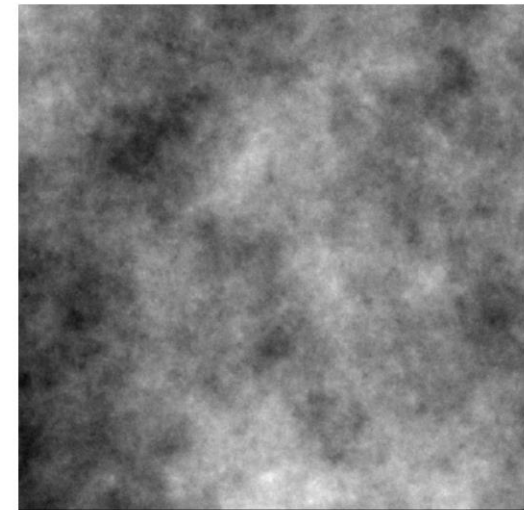
# Fractal Analysis of Grayscale Images: Example



Model FD = 2.20  
Blanket FD = 2.50  
PSA FD = 2.66



Model FD = 2.40  
Blanket FD = 2.57  
PSA FD = 2.67



Model FD = 2.60  
Blanket FD = 2.70  
PSA FD = 2.68

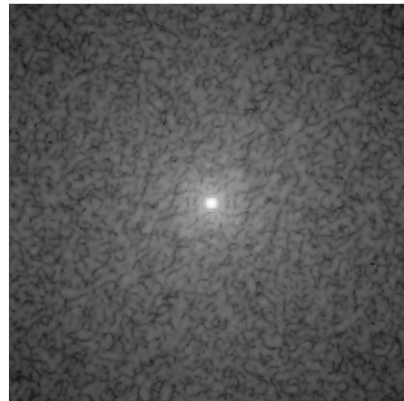


UNIVERSITY OF  
CALGARY

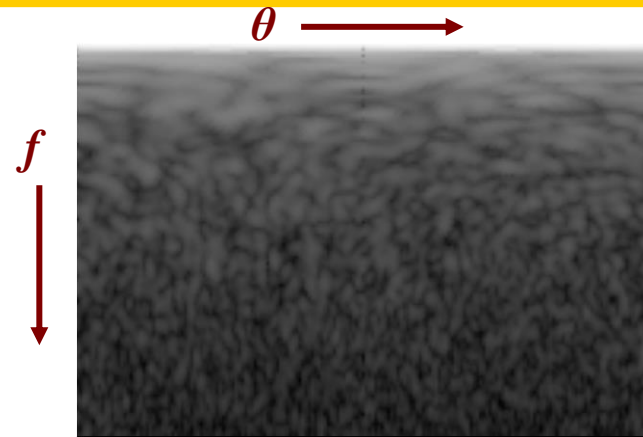
# Fractal and Spectral Analysis of Mammograms



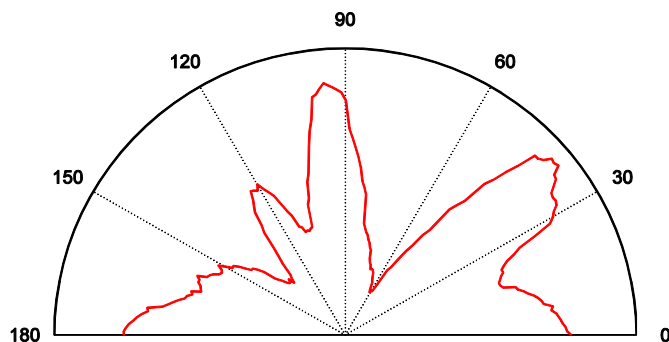
A TP ROI,  $s(x, y)$



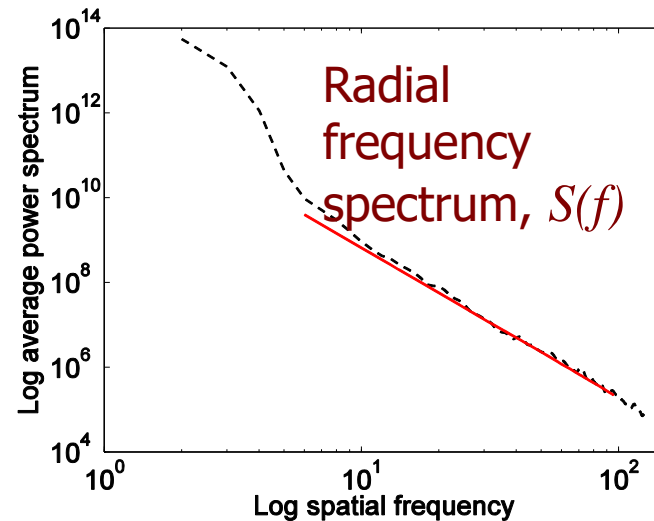
Fourier power spectrum,  $S(u, v)$



Power spectrum in polar coords,  $S(f, \theta)$



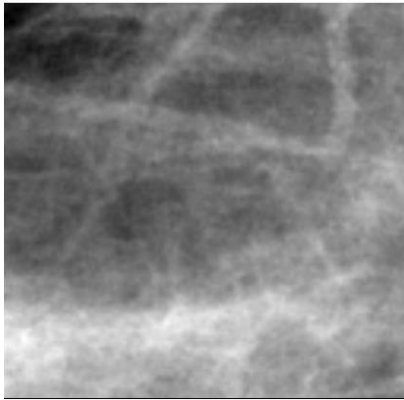
Angular spread of power,  $S(\theta)$



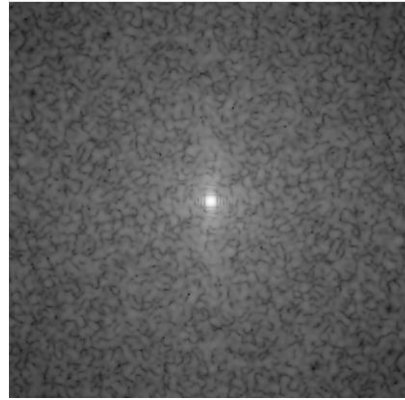


UNIVERSITY OF  
CALGARY

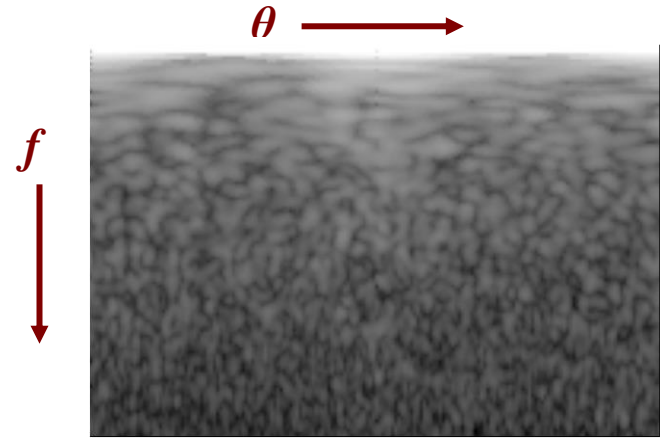
# Fractal and Spectral Analysis of Mammograms



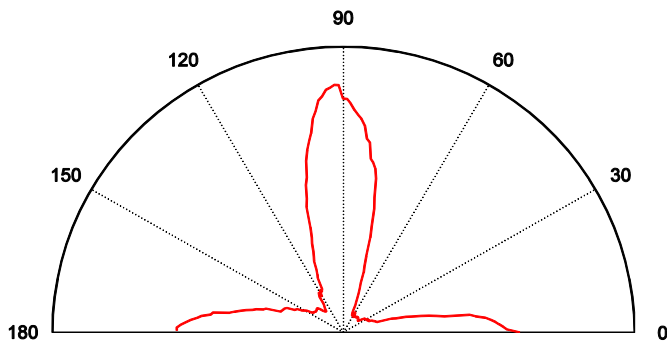
A FP ROI,  $s(x, y)$



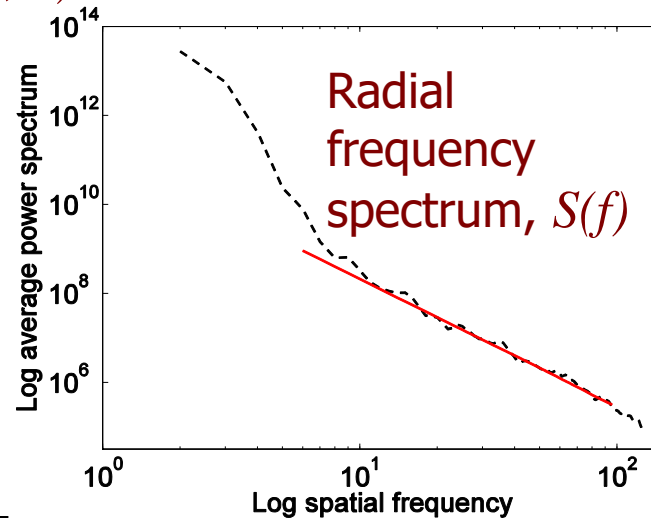
Fourier power  
spectrum,  $S(u, v)$



Power spectrum in  
polar coords,  $S(f, \theta)$



Angular spread of power,  $S(\theta)$



Radial  
frequency  
spectrum,  $S(f)$





UNIVERSITY OF  
CALGARY

# Analysis of Oriented Texture: Sector or Fan Filtering

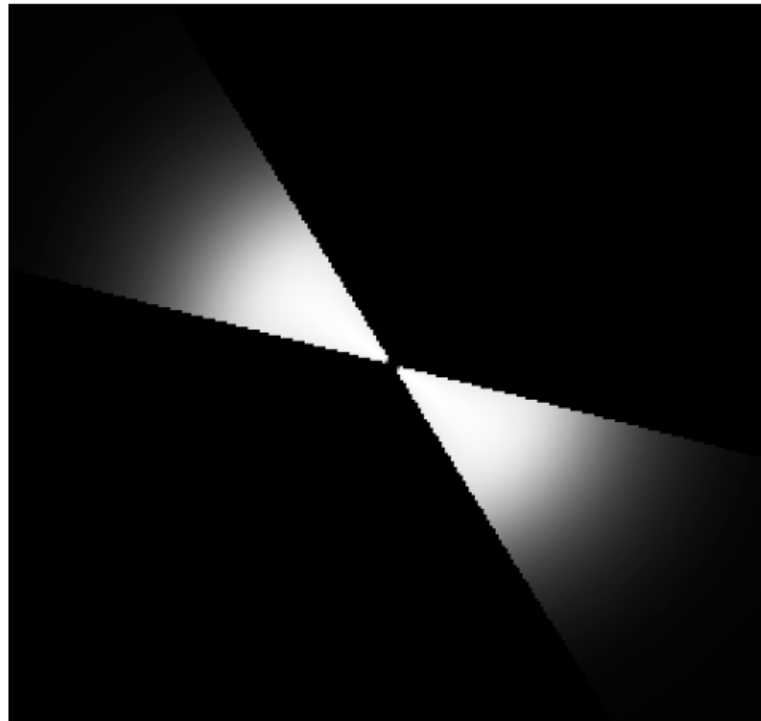
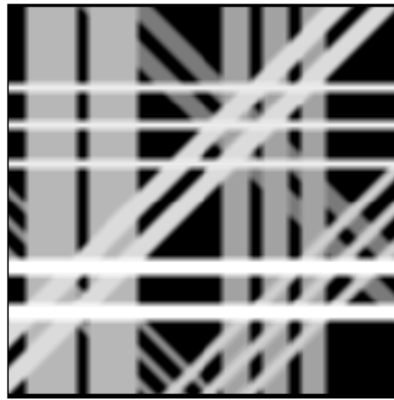
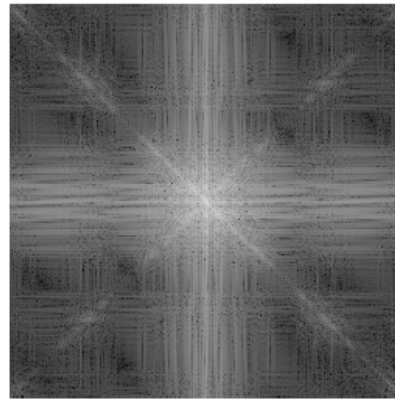


**FIGURE 8.3**

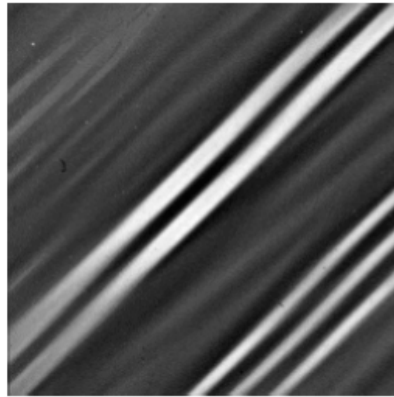
Directional (sector) filter in the Fourier domain. The brightness is proportional to the gain [36]. Figure courtesy of W.A. Rolston [542].



(a)



(b)



(c)



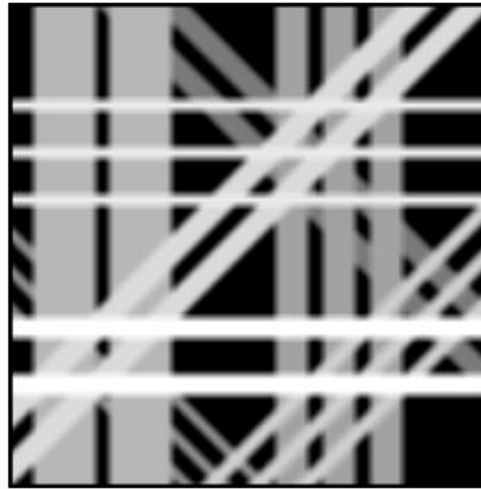
(d)



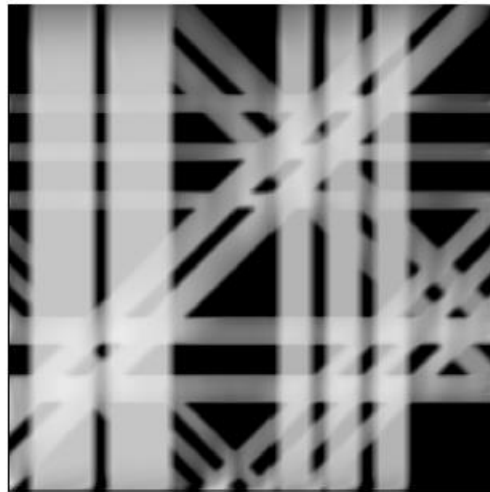
Figure 8.4 (e)



(f)



(a)



(b)



(c)

**FIGURE 8.6**

(a) A test image with overlapping directional components at  $0^\circ$ ,  $45^\circ$ ,  $90^\circ$ , and  $135^\circ$ . Results of fan filtering at  $90^\circ$  after (b) one pass, (c) nine passes. Figure courtesy of W.A. Rolston [542].



# Gabor Filters

The 2D Gabor functions are given as

$$\begin{aligned} h(x, y) &= g(x', y') \exp[-j 2 \pi (U x + V y)], \\ (x', y') &= (x \cos \phi + y \sin \phi, -x \sin \phi + y \cos \phi), \end{aligned} \quad (8.35)$$

where  $(x', y')$  are the  $(x, y)$  coordinates rotated by an arbitrary angle  $\phi$ ,

$$g(x, y) = \left( \frac{1}{2\pi\lambda\sigma^2} \right) \exp \left[ -\frac{(x/\lambda)^2 + y^2}{2\sigma^2} \right] \quad (8.36)$$

is a Gaussian shaping window with the aspect ratio  $\lambda$ , and  $U$  and  $V$  are the center frequencies in the  $(u, v)$  frequency plane.



# Gabor Filter: Impulse Response

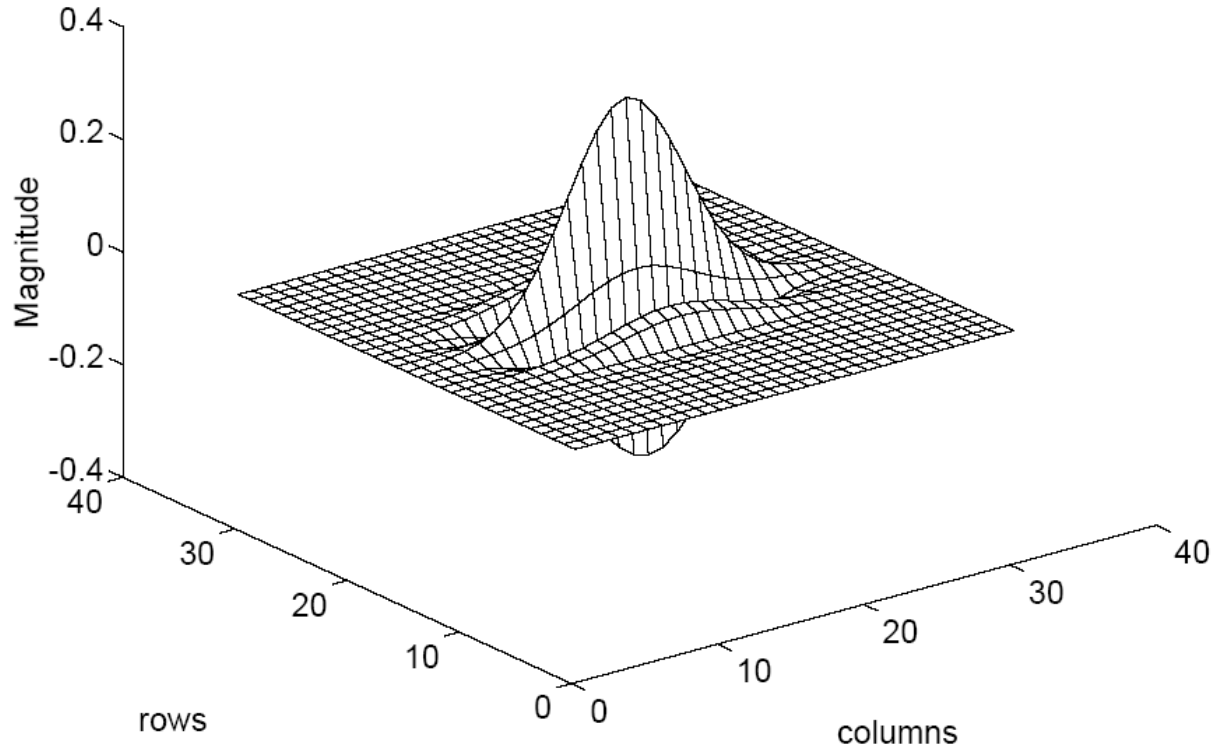


**FIGURE 8.7**

An example of the Gabor kernel with  $\sigma = 0.5$ ,  $\lambda = 0.6$ ,  $U = 1$ ,  $V = 0$ , and  $\phi = 0$  (with reference to Equations 8.35 and 8.36). Figure courtesy of W.A. Rolston [542].



UNIVERSITY OF  
CALGARY

# Gabor Filter: Impulse Response



**FIGURE 8.8**

An example of a Gabor kernel, displayed as an image. Figure courtesy of W.A. Rolston [542].



# Gabor Filter: Frequency Response

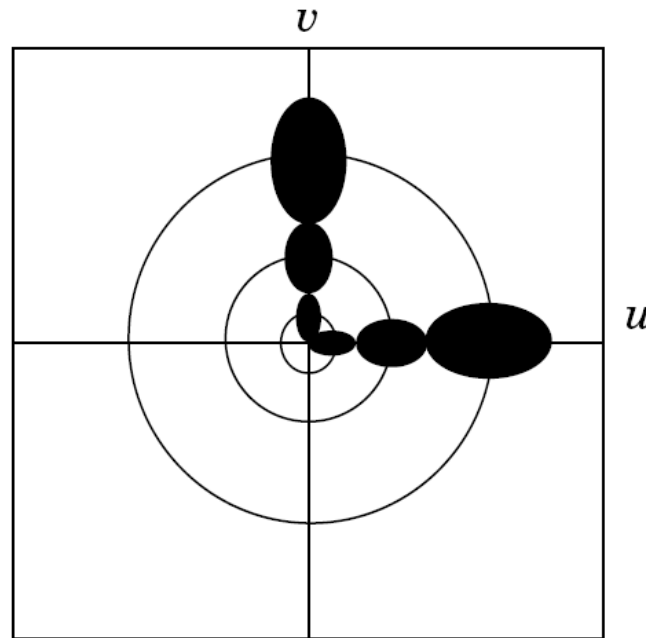
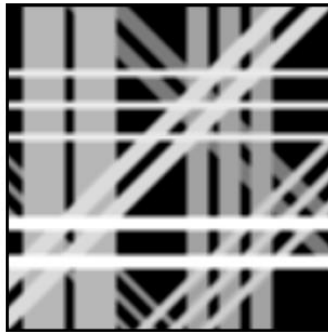
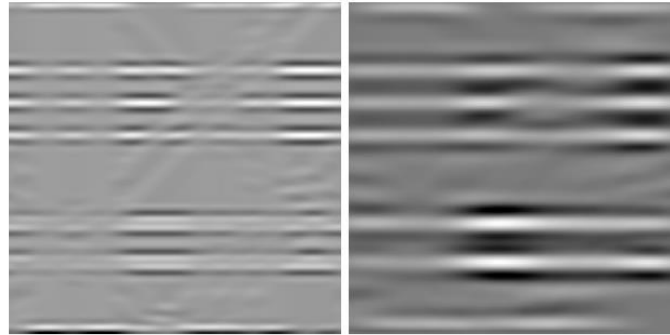


**FIGURE 8.9**

Division of the frequency domain by Gabor filters. Two sets of oval regions are shown in black, corresponding to the passbands of three filters in each set, oriented at  $0^\circ$  and  $90^\circ$ . In each case, the three regions correspond to three scales of the Gabor wavelets. There is a  $90^\circ$  shift between the angles of corresponding filter functions in the space and frequency domains. Figure courtesy of W.A. Rolston [542].

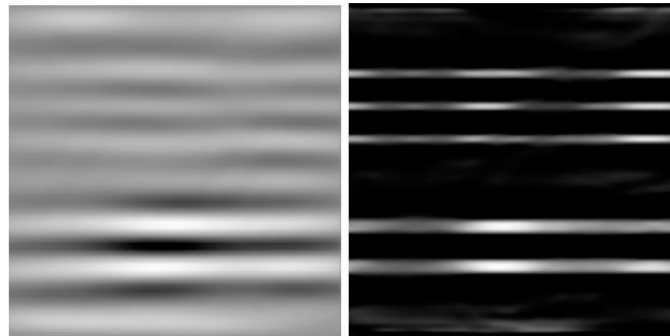


(a)



(b)

(c)



(d)

(e)

**FIGURE 8.11**

(a) A test image with overlapping directional components at  $0^\circ$ ,  $45^\circ$ ,  $90^\circ$ , and  $135^\circ$ . Results of Gabor filtering at  $0^\circ$  after decimation at (b) one-to-one, (c) two-to-one, and (d) four-to-one. (e) Overall response at  $0^\circ$  after vector summation as illustrated in Figure 8.10. Figure courtesy of W.A. Rolston [542].





# Multiscale Analysis with Gabor Filters

$$\psi(x, y) = \frac{1}{2\pi\sigma_x\sigma_y} \exp \left[ -\frac{1}{2} \left( \frac{x^2}{\sigma_x^2} + \frac{y^2}{\sigma_y^2} \right) + j 2\pi W x \right]. \quad (8.73)$$

$$\psi_{m,n}(x, y) = a^{-m} \psi(x', y'), \quad a > 1, \quad m, n = \text{integers}, \quad (8.74)$$

$$x' = a^{-m} [ (x - x_0) \cos \theta + (y - y_0) \sin \theta ],$$

$$y' = a^{-m} [ -(x - x_0) \sin \theta + (y - y_0) \cos \theta ],$$

where  $(x_0, y_0)$  is the center of the filter in the spatial domain,  $\theta = \frac{n\pi}{K}$ ,  $K$  is the total number of orientations desired, and  $m$  and  $n$  indicate the scale and orientation, respectively. The scale factor  $a^{-m}$  in Equation 8.74 is meant to ensure that the energy is independent of  $m$ .

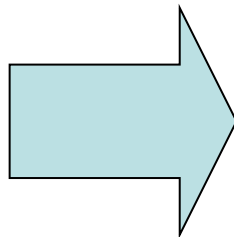


# Gabor Filter: Design Parameters

$$g(x, y) = \frac{1}{2\pi\sigma_x\sigma_y} \exp\left[-\frac{1}{2}\left(\frac{x^2}{\sigma_x^2} + \frac{y^2}{\sigma_y^2}\right)\right] \cos(2\pi f x)$$

## Design parameters

- line thickness  $\tau$
- elongation  $l$
- orientation  $\theta$



## Gabor parameters

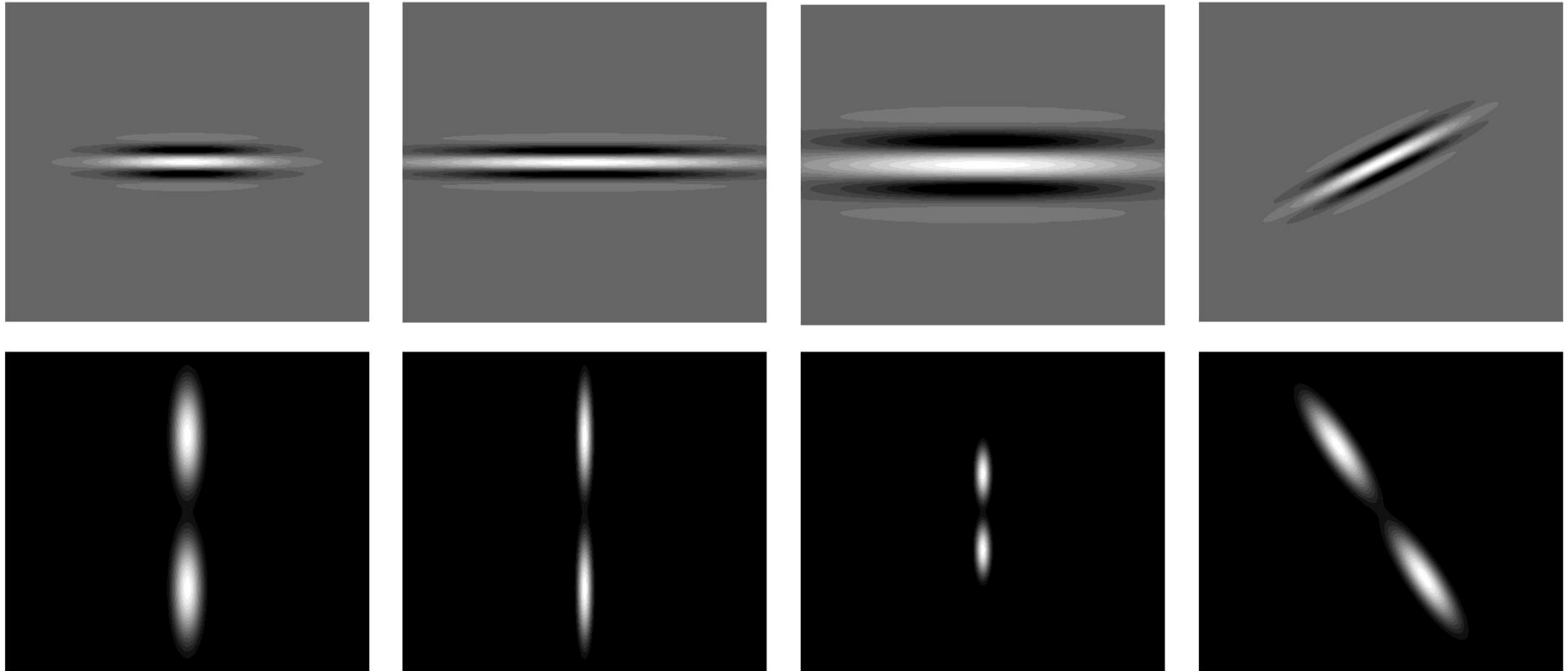
$$f = \frac{1}{\tau}; \quad \sigma_x = \frac{\tau}{2\sqrt{2\ln 2}}$$

$$\sigma_y = l\sigma_x; \quad \begin{bmatrix} x \\ y \end{bmatrix} = \begin{bmatrix} \cos \theta & -\sin \theta \\ \sin \theta & \cos \theta \end{bmatrix} \begin{bmatrix} x' \\ y' \end{bmatrix}$$



UNIVERSITY OF  
CALGARY

# Gabor Filters: Impulse and Frequency Responses





# Multiscale Analysis with Gabor Filters: Frequency Response

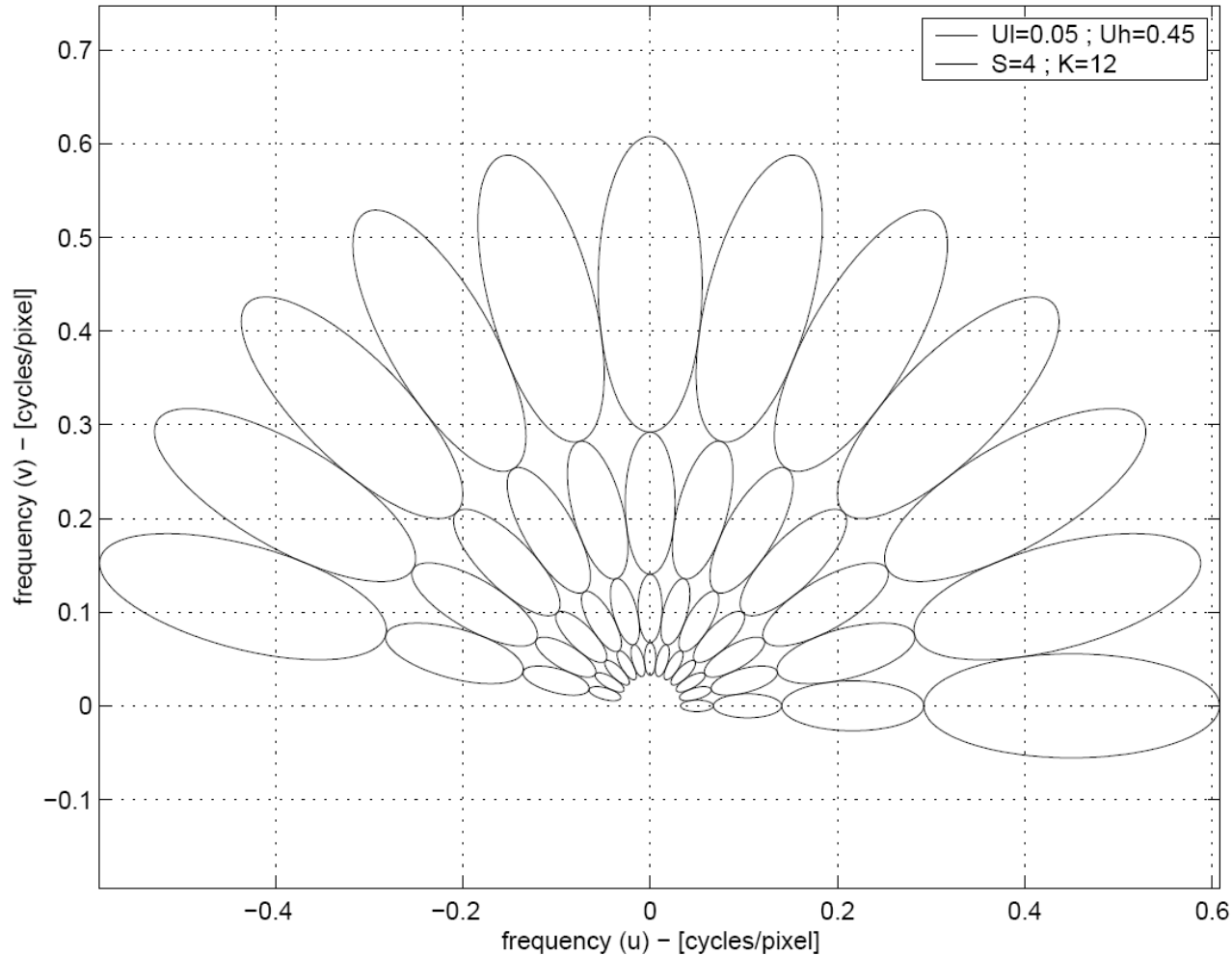
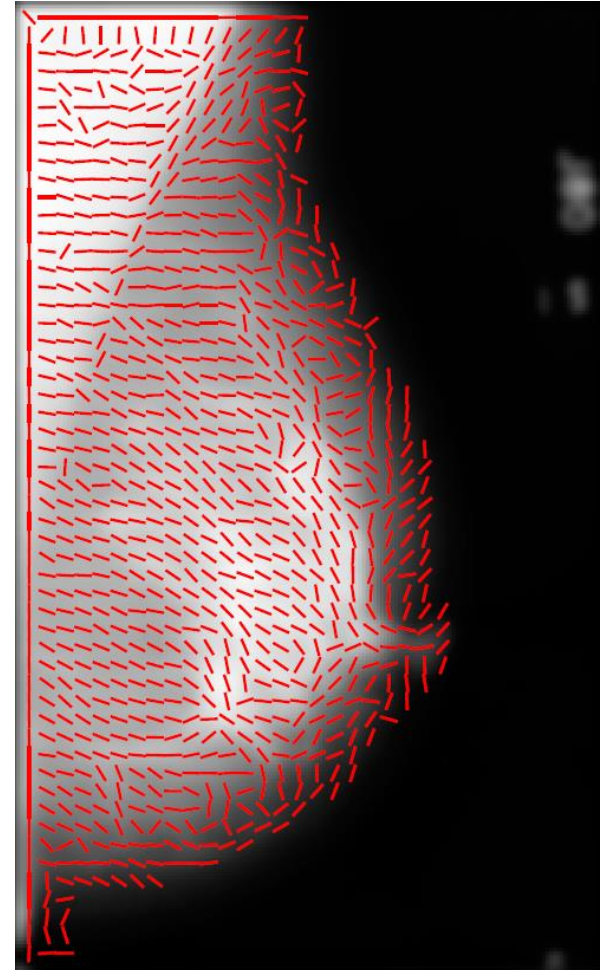
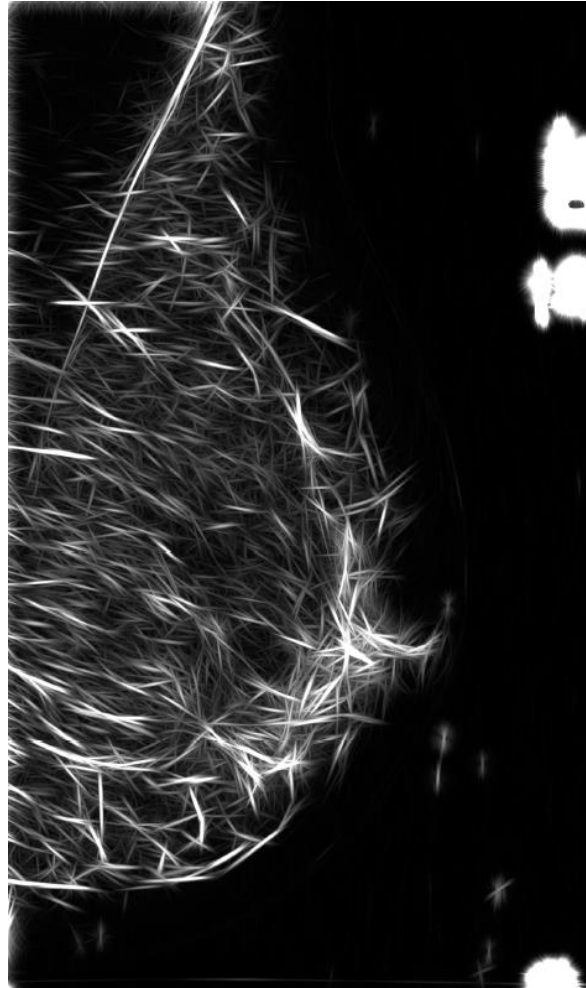
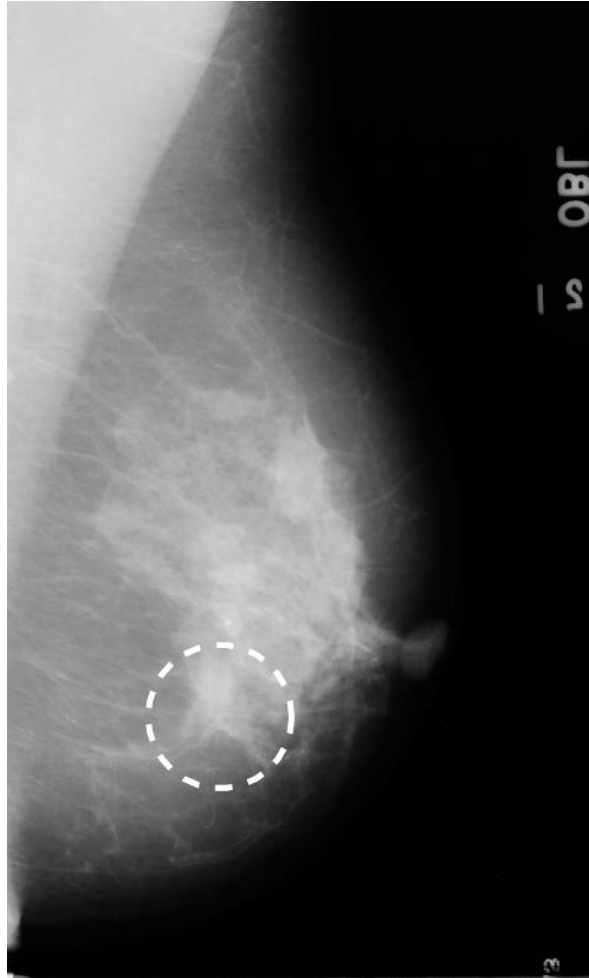


Figure 8.57 (a)



UNIVERSITY OF  
CALGARY

# Gabor Filtering of a Mammogram

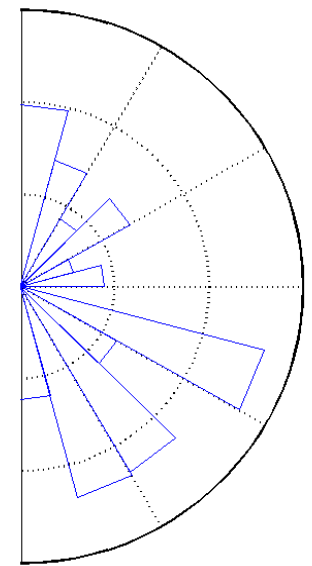
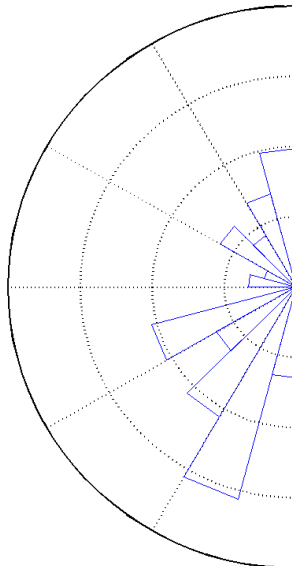
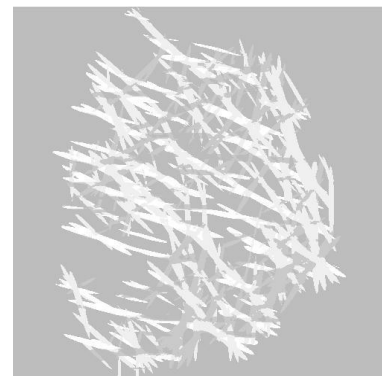
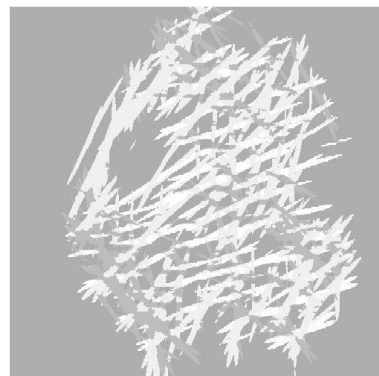
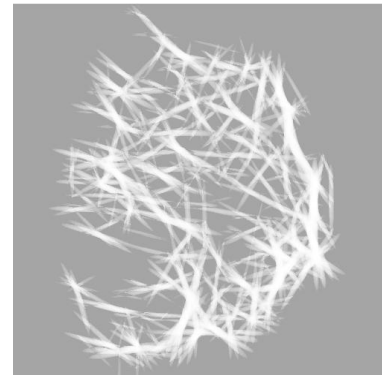
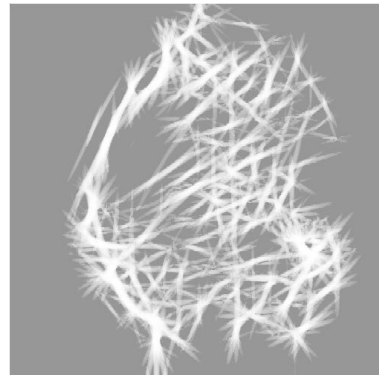
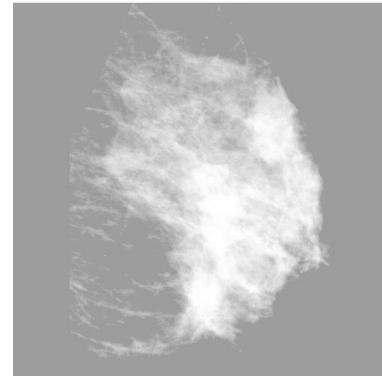
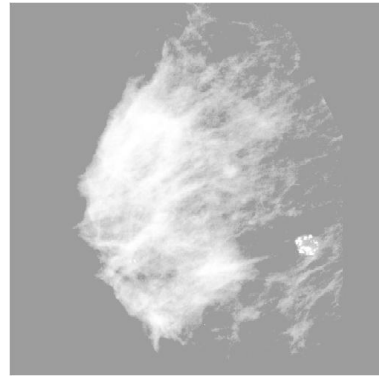


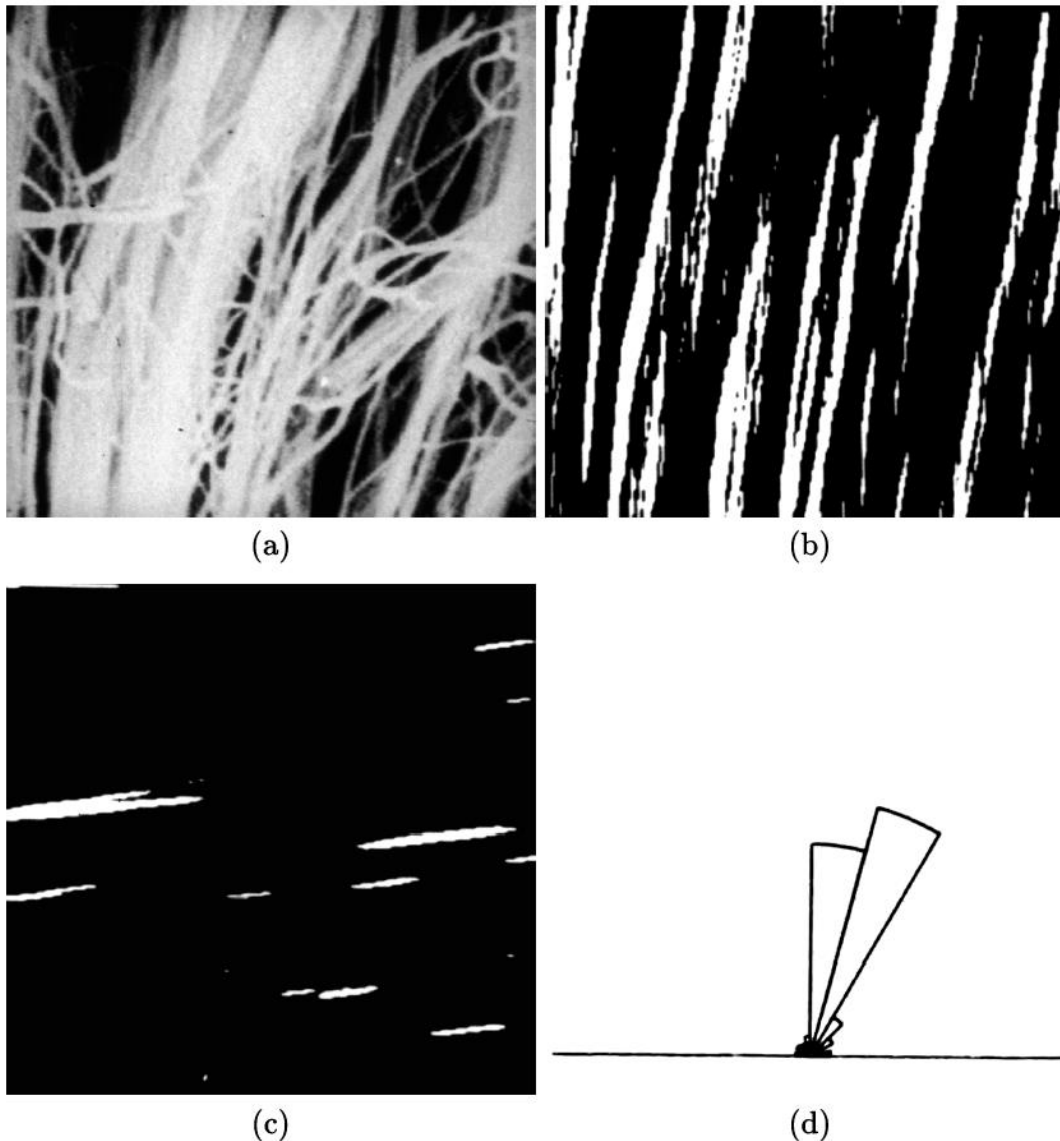


UNIVERSITY OF  
CALGARY

# Analysis of bilateral asymmetry

The directional distribution of fibroglandular tissue differs between the left and right breasts





*Directional  
analysis of  
collagen  
fibers in  
ligaments  
using  
sector or  
fan filters*

**FIGURE 8.20**

(a) A sample image showing collagen alignment in a normal ligament. Binarized directional components in the angle band (b)  $75^\circ - 90^\circ$ , and (c)  $0^\circ - 15^\circ$ . (d) Fractional fiber-covered areas in the form a rose diagram. Figure courtesy of S. Chaudhuri [610].

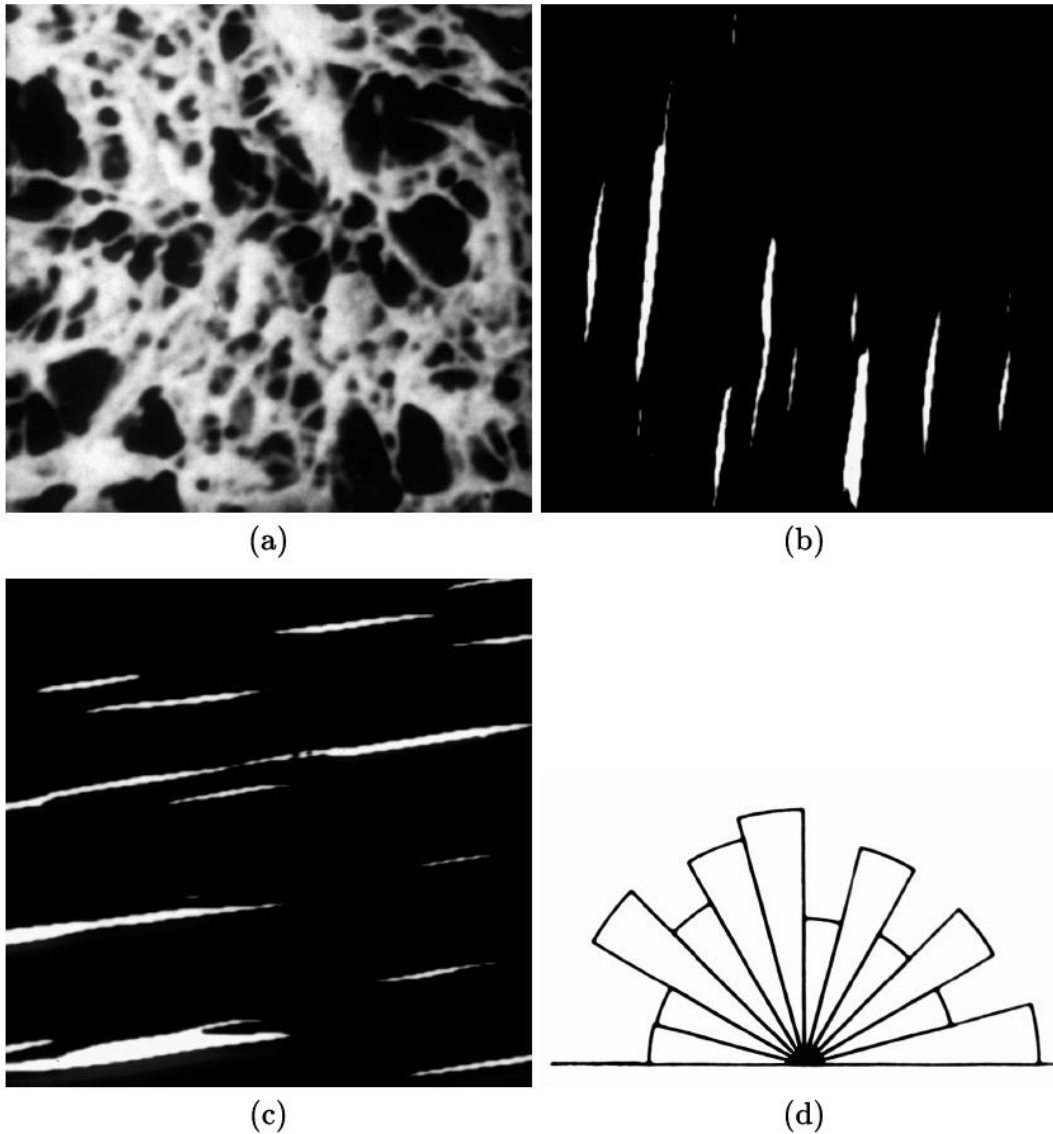


**FIGURE 8.21**

(a) A sample image showing collagen alignment in ligament scar tissue. Binarized directional components in the angle band (b)  $75^\circ - 90^\circ$ , and (c)  $0^\circ - 15^\circ$ . (d) Fractional fiber-covered areas in the form a rose diagram. Figure courtesy of S. Chaudhuri [610].



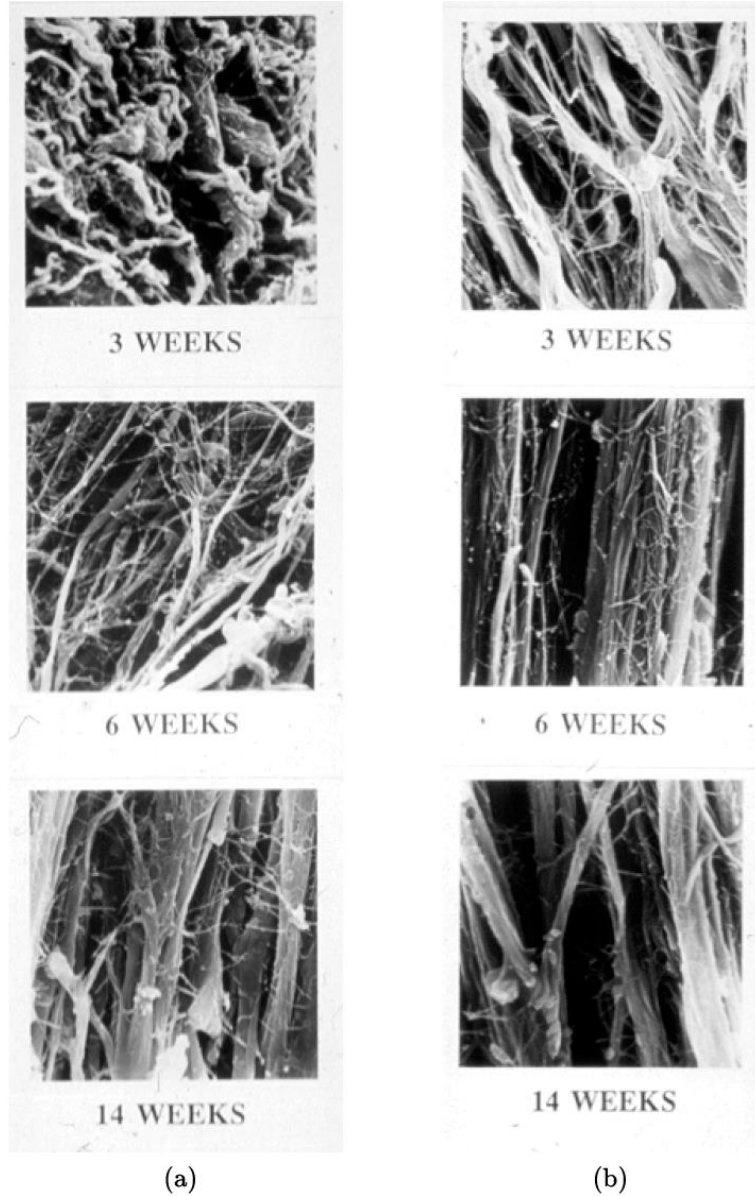
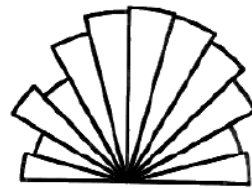


**FIGURE 8.22**

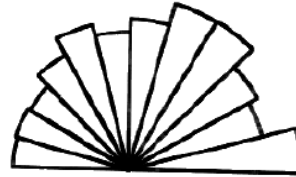
Sample images showing collagen alignment in ligament samples at three weeks, six weeks, and 14 weeks after injury: (a) without immobilization of the affected joint, (b) with immobilization of the affected joint for three weeks. Images courtesy of C.B. Frank. See also Figure 8.23.



3 WEEKS



3 WEEKS



6 WEEKS



6 WEEKS



14 WEEKS



14 WEEKS

(a)

(b)

**FIGURE 8.23**

Composite rose diagrams showing collagen realignment in ligament samples at three weeks, six weeks, and 14 weeks after injury: (a) without immobilization of the affected joint, (b) with immobilization of the affected joint for three weeks. See also Figure 8.22. Reproduced with permission from C.B. Frank, B. MacFarlane, P. Edwards, R. Rangayyan, Z.Q. Liu, S. Walsh, and R. Bray, "A quantitative analysis of matrix alignment in ligament scars: A comparison of movement versus immobilization in an immature rabbit model", *Journal of Orthopaedic Research*, 9(2): 219 – 227, 1991. © Orthopaedic Research Society.

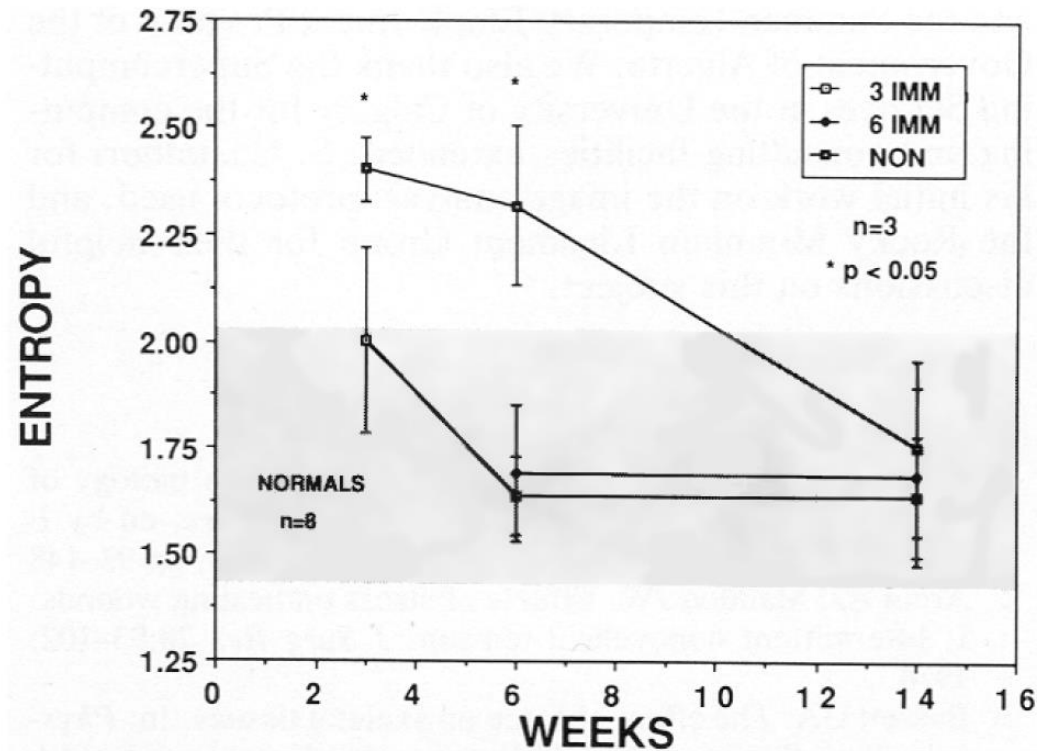


**FIGURE 8.24**

Variation of the entropy of composite rose diagrams with collagen realignment in ligament samples at three weeks, six weeks, and 14 weeks after injury. The vertical bars indicate  $\pm$  one standard deviation about the corresponding means. “NON”: without immobilization of the affected joint; “3 IMM”: with immobilization of the affected joint for three weeks; “6 IMM”: with immobilization of the affected joint for six weeks. The shaded region indicates the range of entropy for normal ligament samples. See also Figures 8.23 and 8.22. Reproduced with permission from C.B. Frank, B. MacFarlane, P. Edwards, R. Rangayyan, Z.Q. Liu, S. Walsh, and R. Bray, “A quantitative analysis of matrix alignment in ligament scars: A comparison of movement versus immobilization in an immature rabbit model”, *Journal of Orthopaedic Research*, 9(2): 219 – 227, 1991. © Orthopaedic Research Society.



# Conclusion

- ❖ Texture and fractal analysis of biomedical images can provide useful features for computer-aided diagnosis



UNIVERSITY OF  
CALGARY

# Thank you!

- ❖ Natural Sciences and Engineering Research Council of Canada
- ❖ My collaborators and students

<http://people.ucalgary.ca/~ranga/enel697/>

